Earth-science Reviews
August 2013, Volume 123 Pages 173-193
https://doi.org/10.1016/j.earscirev.2013.04.006
https://archimer.ifremer.fr/doc/00264/37510/

Pleistocene sea-surface temperature evolution: Early cooling, delayed glacial intensification, and implications for the mid-Pleistocene climate transition.

McClymont Erin L. [1, *], Sosdian Sindia M. [2], Rosell-Mele Antoni [4, 5], Rosenthal Yair [2, 3]

[1] Newcastle Univ, Sch Geog Polit & Sociol, Newcastle Upon Tyne NE1 7RU, Tyne & Wear, England.
[2] Rutgers State Univ, Inst Marine & Coastal Sci, New Brunswick, NJ 08901 USA.
[3] Rutgers State Univ, Dept Geol, New Brunswick, NJ 08901 USA.
[4] Univ Autonoma Barcelona, Inst Ciencia & Tecnol Ambientals, Bellaterra 08193, Catalonia, Spain.
[5] ICREA, Barcelona 08010, Catalonia, Spain.

Corresponding author email address : erin.mcclymont@durham.ac.uk

SosdianS@cardiff.ac.uk ; antoni.rosell@uab.cat ; rosentha@marine.rutgers.edu

Abstract :

mid-Pleistocene climate transition (MPT) is defined by the emergence of high amplitude, quasi-100 ka glacial-interglacial cycles from a prior regime of more subtle 41 ka cycles. This change in periodicity and amplitude cannot be explained by a change in 'external' astronomical forcing. Here, we review and integrate published records of sea-surface temperatures (SSTs) to assess whether a common global expression of the MPT in the surface ocean can be recognized, and examine our findings in light of mechanisms proposed to explain climate system reorganization across the MPT. We show that glacial-interglacial variability in SSTs is superimposed upon a longer-term cooling trend in oceanographic systems spanning the low-to high-latitudes. Regional variability exists in the timing of the onset and magnitude of cooling but, in most cases, a long-term cooling trend begins or intensifies from similar to 1.2 Ma (Marine Isotope Stage, MIS, 35-34). The SST cooling accompanies a long-term trend towards higher global ice volume as recorded in benthic foraminifera delta O-18, but predates a step-like increase in delta(18)Oat similar to 0.9 Ma (MIS 24-22) that is argued to reflect expansion of continental ice-sheets. The strongest expression of Pleistocene cooling is found during glacial stages, whereas minor or negligible trends in interglacial temperatures are identified. However, pronounced cooling during both glacial and interglacial maxima is evident at 0.9 Ma. Alongside the long-term SST cooling trends, quasi-100 ka cycles begin to emerge in both the SST and delta O-18 records at 1.2 Ma, and become dominant with the expansion of the ice-sheets at 0.9 Ma. We show that the intensified glacial-stage cooling is accompanied by evolving pCO(2), abyssal ocean ventilation, atmospheric circulation and/or dust inputs to the Southern Ocean. These changes in diverse environmental parameters suggest that glacial climate boundary conditions evolved across the MPT. In turn, these modified boundary conditions may have altered climate sensitivity to orbital forcing by placing pre-existing ice-sheets closer to some threshold of climate-ice sheet response.

Keywords : Sea surface temperatures, Mid-Pleistocene transition, Ice sheets, 100 kyr world

1. INTRODUCTION

Records of mid and late Pleistocene climate are characterized by the emergence and subsequent dominance of large amplitude, asymmetric ('saw-tooth') quasi-100 ka glacial-interglacial cycles. This pattern contrasts with the early Pleistocene dominance of smaller amplitude ~41 ka glacial cycles. The transition from the 41 ka to 100 ka climate cycles is termed the "mid-Pleistocene climate transition" (MPT). In the absence of any noteworthy shifts in the strength of orbital variations (Laskar et al., 2004), the shift in glacial cycle periodicity suggests that the climate system developed an enhanced sensitivity to orbital forcing across the MPT (Imbrie et al., 1993; Ravelo et al., 2004). Debate continues regarding the nature of the climatic feedbacks and teleconnections involved in this transition. A step-wise increase in benthic foraminifera $\delta^{18}O$ (Mudelsee and Schulz, 1997) has been interpreted to indicate larger northern hemisphere ice-sheets, whose inertia relative to insolation forcing may account for the subsequent dominance of comparatively long quasi-100 ka cycles by 0.6 Ma (Clark and Pollard, 1998; Imbrie et al., 1993; Mudelsee and Schulz, 1997). More recently, however, it has

been argued for an increase in Antarctic ice volume as the cause of the rapid and stepped increase in seawater $\delta^{18}O$ at 0.9 Ma (Elderfield et al., 2012; Pollard and DeConto, 2009). However, other key climate system components began to evolve prior to a change in the frequency of the waxing and waning of the ice-sheets. Events of significance include the intensification of tropical Pacific ocean/atmosphere circulation (e.g. de Garidel-Thoron et al., 2005; McClymont and Rosell-Melé, 2005; Medina-Elizalde and Lea, 2005), cooling and expansion of subarctic and polar water masses in the Pacific, Atlantic and Southern Oceans (Lawrence et al., 2011; Martinez-Garcia et al., 2010; McClymont et al., 2008; Rodríguez-Sanz et al., 2012), cooling in upwelling systems (Dekens et al., 2007; Etourneau et al., 2009; Lawrence et al., 2006; Marlow et al., 2000), cooling in the deep Atlantic ocean (Sosdian and Rosenthal, 2009), evolving Asian monsoon strength (Heslop et al., 2002; Sun et al., 2006), and perturbations to thermohaline circulation (Schmieder et al., 2000; Sexton and Barker, 2012). These events also provide the climatic context within which biological evolutionary events occur in the oceans (Hayward et al., 2007) and on land, including in the hominid record (de Menocal, 2004; Head and Gibbard, 2005).

Proposed mechanisms to account for these transitions in Pleistocene climate history include a threshold response to longer-term atmospheric CO_2 decline (e.g. Berger and Jansen, 1994; Raymo, 1997). This hypothesis is frequently invoked despite the limited availability of Pliocene and Pleistocene atmospheric CO_2 records prior to the oldest Antarctic ice core data, currently at ~0.8 Ma (Bartoli et al., 2011; Hönisch et al., 2009; Luthi et al., 2008; Seki et al., 2010). Furthermore, biogeochemical modeling and comparison to a stacked marine stable carbon isotope record questions the evidence for a long-term CO_2 decline over the last 1.2 Ma (Hoogakker et al., 2006). Recent pCO_2

reconstructions do not show a long-term decline during the Pleistocene, but suggest that glacial values prior to ~1 Ma were 30±30 μatm higher than the late Pleistocene (Hönisch et al., 2009). In contrast, estimated interglacial pCO_2 values before the MPT are statistically the same as those of the late Pleistocene, with a temporary reduction in interglacial pCO_2 between 1 and 0.6 Ma (Hönisch et al., 2009). Although small, these reductions in glacial pCO_2 might have been sufficient to encourage intensification of glacial stages if they were associated with changing climate sensitivity and/or climate feedbacks such as the ice-albedo feedback (Van de Wal and Bintanja, 2009).

Other proposals to explain Pleistocene climate evolution argue for changing ice-sheet dynamics in the northern hemisphere and/or on Antarctica as key (Clark and Pollard, 1998; Crowley and Hyde, 2008; Raymo et al., 2006). Feedbacks related to deep-water cooling, thermocline depth, sea-ice distributions, and atmospheric circulation are also invoked to explain Pleistocene climate evolution (Lee and Poulsen, 2006; McClymont and Rosell-Melé, 2005; Tziperman and Gildor, 2003). These hypotheses consider both the observed teleconnections between low and high latitudes, and the direct impacts of ocean circulation change on ice-sheet growth via potential influences on air temperatures and snowpack development in the ice sheet source regions. Whilst there is growing evidence for changing ocean/atmosphere circulation pre-dating, and accompanying, ice-sheet expansion (e.g. de Menocal, 1995; Heslop et al., 2002; Liu and Herbert, 2004; Marlow et al., 2000; McClymont and Rosell-Melé, 2005; McClymont et al., 2008; Medina-Elizalde and Lea, 2005; Sexton and Barker, 2012) it is not clear whether this was effective in driving climate changes which were conducive to the emergence of longer, higher amplitude 100 ka ice volume cycles. It is also possible that the proposed northern hemisphere ice-sheet expansion was controlled

by glaciological factors including erosion of the basal substrate and its impacts over ice-sheet duration and stability (Clark et al., 2006). An evolving climate response to orbital variability has also been proposed, including an increasingly non-linear response to obliquity pacing (Huybers, 2007), which may relate to changing carbon cycle / Antarctic temperature / radiative forcing relationships (Masson-Delmotte et al., 2010). A combination of obliquity and precession feedbacks on CO_2 and albedo have been argued to drive both the growth and decay of the large northern hemisphere ice-sheets on orbital timescales (Ruddiman, 2006); the appearance of the MPT may imply that these orbitally-paced feedbacks changed during the Pleistocene.

Compilations of marine, ice core and terrestrial evidence have highlighted an increase in interglacial temperatures after the "Mid Brunhes Event" (MBE) at ca. 430 ka (Lang and Wolff, 2011; Masson-Delmotte et al., 2010; Jouzel et al., 2008; Elderfield et al., 2012; Lawrence et al., 2006, 2009; Martinez-Garcia et al., 2010), when interglacial CO_2 concentrations also increase (Hönisch et al., 2009; Lang and Wolff, 2011; Masson-Delmotte et al., 2010). Although the global expression of these events has been questioned (Candy et al., 2010), the "warm" late Pleistocene interglacials observed in many records (e.g. Antarctic ice cores, lower abyssal Pacific, SSTs in the Southern, N. Pacific, N. Atlantic and E. Pacific oceans) are also difficult to explain as a direct response to regular orbital forcing, and emphasise the existence of additional feedbacks such as greenhouse gas forcing (Yin and Berger, 2010), ice-sheet albedo and thermohaline circulation (Lang and Wolff, 2011; Masson-Delmotte et al., 2010). An intriguing possibility is also that the intensity of the preceding glaciation may play a role in the subsequent interglacial warmth, thus making predictions of interglacial strength a challenge using orbital forcing alone (Lang and Wolff, 2011). These new

insights indicate that the climate system response to orbital forcing may have continued to evolve during, or following, the later stages of the MPT.

To assess and evaluate the proposed driving mechanisms for the MPT in the context of Pleistocene climate evolution requires the resolution of a number of issues. Specifically, it is unclear whether the MPT was a globally synchronous transition, or if it was time-transgressive and propagated through a suite of key systems and feedbacks. For example, early work suggested both the onset and duration of the MPT to vary between 1.1 Ma-0.4 Ma (Ruddiman et al., 1986). In contrast, a synthesis of benthic $\delta^{18}O$ time-series detected a comparative uniformity in the onset of the MPT at 0.9-0.6 Ma (1997), yet another synthesis places the MPT at 1.2 – 0.7 Ma (Clark et al., 2006). Here, we review new and previously published evidence for SST evolution through the Pleistocene in order to answer the following questions: (i) do globally distributed SST records display a common cooling trend across the MPT? (ii) did SSTs change gradually or abruptly? (iii) did global SSTs change synchronously, or do regional overprints exist? (iv) did glacial-interglacial SST cycles become more intense across the MPT? (v) did a shift in the period of glacial-interglacial SST cycles occur?

Our new, and the previously published, SST records allow us to assess the magnitude of surface ocean temperature change in several key oceanographic systems. SSTs reflect both radiative heating and the redistribution of heat via local and regional ocean and atmosphere circulation patterns. Thus, differences between SST records give insight into regional trends whereas common trends across multiple locations may be indicative of a 'global' transition. Here we re-analyze published SST data spanning the MPT in order to calculate the magnitude of SST change, to constrain the timing of its onset, and test for the possibility of a co-ordinated response in glacial/interglacial

variability (including in the spectral domain). Records are compared from 26 sites (Figure 1, Table 1) each of which is of a resolution appropriate for the detection of orbital variability and have astronomically calibrated age models. The SST records have been generated using the alkenone-derived proxy, U^{K}_{37}' (Brassell et al., 1986; Müller et al., 1998; Prahl et al., 1988), Mg/Ca ratios in planktonic foraminifera (Anand et al., 2003; Lea et al., 1999; Lea et al., 2000), or transfer function outputs from planktonic foraminifera assemblages (Imbrie and Kipp, 1971; Kucera et al., 2005; Vincent and Berger, 1981).

Data sets have been processed in several ways, to determine: (i) the presence of statistically significant long-term trends in the mean, interglacial, and glacial states; (ii) the evolution of the dominant periodicities expressed in each record; (iii) changes in the amplitudes of glacial/interglacial variability. This is the first comprehensive analysis of long-term trends and spectral properties of SST records spanning the MPT, drawing on sites that span both low and high latitudes, and that represent a wide range of oceanographic regimes. In section 2 we describe the proxies and sites which we have reviewed. Section 3 highlights the statistical treatments we have employed. Section 4 focuses on the regional expressions of SSTs, while Section 5 assesses the global features of the records and implications for an improved mechanistic understanding of the MPT.

2. SEA-SURFACE TEMPERATURE (SST) PROXIES

The three proxies utilized here are all calibrated against modern SST, but the mechanisms by which temperature is recorded, preserved and interpreted differ among

techniques. For all three proxies, we apply SST calibrations developed using sediment core-tops, which take into account the potential impacts of processes affecting the sedimentary record, such as degradation and dissolution within the water column and the averaging of seasonal signals.

2.1 The alkenone U^{K}_{37}' index

The U^{K}_{37}' index describes the relative distributions of two C_{37} alkenones (Prahl and Wakeham, 1987) biosynthesized by some Haptophyceae algae, including the dominant coccolithophorids in the modern ocean, *Emiliania huxleyi* and *Gephyrocapsa oceanica* (Conte et al., 1995; Marlowe et al., 1990; Prahl et al., 1988; Volkman et al., 1995; Volkman et al., 1980):

$$U^{K}_{37}' = [C_{37:2}] / [C_{37:2} + C_{37:3}]$$

Global core-top U^{K}_{37}' values are significantly correlated to mean annual SSTs, with a mean standard error of estimation of 1.1°C (Conte et al., 2006; Müller et al., 1998), demonstrating sedimentary integration of spatial and temporal variability in surface ocean production and thus in the algal growth temperature during alkenone synthesis. Alkenone degradation within the water column and sediments does not distort the U^{K}_{37}' index (e.g. Conte et al., 1992; Sawada et al., 1998), and Pleistocene evolutionary events in coccolithophorids appear not to affect the U^{K}_{37}' relationship to SST (McClymont et al., 2005). Due to concerns regarding the quantification of SST in the Nordic Seas in the presence of high (>5%) concentrations of the $C_{37:4}$ alkenone (Bendle and Rosell-Melé, 2004), we use the U^{K}_{37} results from Site 983 in the northern North Atlantic (McClymont et al., 2008). An alkenone SST record from site 806 is not

included here, since a continuous record could not be achieved due to SSTs often exceeding the upper limit of the proxy (McClymont and Rosell-Melé, 2005).

2.2 Mg/Ca in planktonic foraminifera

The Mg content of foraminiferal calcite, expressed as Mg/Ca, reflects the biologically mediated but temperature-dependent substitution of Mg for Ca into calcite (Rosenthal, 2007):

$$Mg / Ca \text{ (mmol mol-1)} = Be^{AT}$$

A temperature sensitivity of ~9% change in Mg/Ca per degree Celsius is indicated by published 'A' values of 0.09±0.01 $°C^{-1}$ (Anand and Elderfield, 2003; Dekens et al., 2002; Rosenthal and Lohmann, 2002). Species-specific effects are primarily expressed by the range of pre-exponential constants ('B') from 0.31-0.52 (Dekens et al., 2008) which determine absolute temperature calculations (Rosenthal, 2007). Bias may be introduced due to preferential loss of Mg by dissolution of Mg-rich calcite (e.g. Brown and Elderfield, 1996; Rosenthal et al., 2000) but can be corrected for by using estimates of carbonate ion concentration (Dekens et al., 2002). Variations in seawater Mg/Ca also need to be considered when estimating secular changes in ocean temperature from foraminiferal Mg/Ca. However, available reconstructions suggest very minor change in seawater Mg/Ca over the Pleistocene (past ~2 Ma) (Fantle and DePaolo, 2006; Sime et al., 2007), consistent with the long oceanic residence times (>1 Myr) of these major elements. A comparison of U^{K}_{37}' and Mg/Ca SST reconstructions spanning the last 5 Ma in the east Pacific did not identify any significant offsets between the two proxies that could be linked to changing seawater Mg/Ca ratios (Dekens et al., 2008). The same

study showed, through propagation of the errors associated with the issues outlined above, that the range of uncertainty in absolute Mg/Ca-derived SSTs may be around 1.7 °C (Dekens et al., 2008).

2.3 Transfer functions in planktonic foraminifera

Transfer functions seek to quantify the environmental variables that determine the assemblages of planktonic foraminifera, including SST, salinity and thermocline depth (Imbrie and Kipp, 1971; Jian et al., 2000; Kucera et al., 2005). Core-top calibrations are the preferred method of transfer function generation, as they incorporate temporal and spatial variability in production and diagenetic impacts upon initial sedimentation (Kucera et al., 2005). The three transfer function data sets used here are those used in the original publications (Table 1): the Imbrie-Kipp (1971) method based on Atlantic core-tops for Site 607 (Ruddiman et al., 1989), the FP-12E function from the western north Pacific (Thompson, 1981) for Site GIK17957-2 (Jian et al., 2000), and an artificial neural network (ANN) technique for Site 1143 (Crundwell et al., 2008). Of importance for all applications of transfer function proxies is the potential for non-analogue situations to arise as a result of evolutionary events within the foraminiferal assemblage, particularly prior to 1 Ma (Kucera et al., 2005). For example, the early Pleistocene contains a number of adaptations to habitat changes (e.g. changes to the morphology of *Neogloboquadrina pachyderma* in the Pacific c. 1 Ma, Kucera & Kennett, 2002). The benthic foraminifera record, although not used here for quantitative temperature reconstructions, also contains a suite of extinction events argued to be

associated with circulation change across the MPT (Kawagata et al., 2005). The potential impacts of such events are considered below.

3. METHODS

Site selection for our compilation was determined by the availability of a continuous (sample resolution <50 ka) record of absolute SSTs spanning the MPT, chronologically constrained by either astronomical calibration (using $\delta^{18}O$ or saturated bulk density of the sediment) or detailed biostratigraphy (Table 1). The highest resolution records are 2-3 ka while the lowest resolution records tend towards ~50 ka. Whilst other SST records are available that span parts of the Pleistocene, they were not included in this study where one or more of these criteria were not met.

3.1 Sea-surface temperature calculations

Alkenone-derived SST records are presented from 12 ODP sites (Table 1), including unpublished data from Site 1081 and 1087 in the Benguela system (Petrick et al., in prep.; Rosell-Melé et al., under review). All SST calculations are using the global core-top U^{K}_{37}' calibration of Müller et al. (1998). Sites 607, 982 and 1077 (Lawrence et al., 2009; Schefuß et al., 2004) are previously published records which did not use this calibration. To ensure consistency between sites we re-calculated SSTs for Sites 607, 982, and 1077 using the Müller calibration. This resulted in a small change to absolute SSTs for these sites in the range of -0.19 to +0.15°C.

Five Mg/Ca-derived SST records are presented, based on measurements of *Globigerinoides ruber* and *G. sacculifer* (Table 1). For Site 806, two different records are presented, which differ in the species utilized and sampling resolution (Medina-Elizalde and Lea, 2005; Wara et al., 2005). Conversion of Mg/Ca to absolute SST may be affected by the species analyzed, potential $CaCO_3$ dissolution, the size fraction analyzed and the cleaning method used prior to analysis (e.g. Barker et al., 2005; Dekens et al., 2002). We use the absolute SST records produced by the original authors, which take these site/lab specific issues into account. We also acknowledge that even if these processes might result in subtly different absolute estimated SSTs, the sensitivity of Mg/Ca to temperature change is more or less similar as expressed in co-efficient "A" discussed above. Therefore, the magnitude and timing of the SST changes we seek to quantify remain robust.

The planktonic foraminifera transfer function records are presented as originally published (Crundwell et al., 2008; Jian et al., 2003; Ruddiman et al., 1989), in recognition of the regional calibrations used and the absence of non-analogue situations that might introduce increased uncertainties into the calibrations. Evolutionary effects on all three records appear to be minor. At Site 1123, the ANN-25 transfer function removes taxa which emerge and/or largely disappear through the Pleistocene (*Truncorotalia truncatulinoides* (S) and *Tr. crassula*; Crundwell et al., 2008), and Ruddiman *et al.* (1989) could not distinguish whether the absence of the polar foraminifera *N. pachyderma* (s.) between 1.25 and 1.1 Ma at ODP607 was the result of climate or evolutionary factors. A recently published alkenone-derived SST record from the same site (Lawrence et al., 2011) depicts both the same absolute SSTs and timing of SST change as the foraminifera transfer function data; however, we use the ODP607

alkenone record in this compilation given the concern about evolutionary events impacting the foraminifera transfer function data set.

3.2 Age models

All time-series are presented using the previously published age models (Table 1), which were tuned to either the benthic $\delta^{18}O$ record of ODP 677 (Shackleton et al., 1990) or to the benthic $\delta^{18}O$ stack, LR04 (Lisiecki and Raymo, 2005). The difference between the chronologies is <7 ka during the interval studied here, with a maximum age offset of 10 ka magnetic polarity reversal datums during the last 2 Ma (Lisiecki and Raymo, 2005). Lower resolution shipboard biostratigraphies constrain several sites (Table 1). The uncertainties in the chronological frameworks used here do not affect our interpretations of the timing of long-term (>orbital-scale) trends, but could impact on the identification of orbital-scale variability. We therefore limit our spectral analyses to sites with orbitally-calibrated chronologies.

We also note here that as per international convention (ISO 31), we here use the terms ka and Ma (kiloannum, million annum) to signify both the age of an event in thousands and millions of years before present, and also the duration of an event or cycle. The latter is more commonly referred to by kyr or Myr e.g. the MPT is often described as the transition from the "41 kyr world" to the "100 kyr world", but is here referred to as a transition from 41 ka to 100 ka cycles.

3.3 Statistical treatments

3.3.1 Long-term trends in temperature

In order to identify long-term trends that are not associated with orbital-scale variations, a series of low-bandpass filters was applied to each record (Trauth, 2007) which act to suppress all frequencies above the cut-off frequency. For example, a 200 ka low-bandpass filter will remove or suppress precession, obliquity and 100 ka eccentricity-related components. To test for whether these trends were significantly different to the null hypothesis of "no trend", we employed the SiZer programme (Chaudhuri and Marron, 1999). This process fits a series of smoothed curves to the data at a series of bandwidths, and tests each curve for deviation away from zero. In addition, SiZer details when data is too sparse to make a definitive conclusion. The resulting "SiZer map" indicates the regions where there are significant trends (or not) through the time series, for each of those bandwidths. Thus, this approach allows trends to be determined, assessed, and considered with respect to the bandwidth at which these are most clearly expressed. Previous work employing different bandwidths for benthic $\delta^{13}C$ records has shown that changes in the cut-off frequency which is employed can lead to alteration in the apparent timing of global trends by up to 20 ka (Hoogakker et al., 2006). We also note that variation in the timing of events can differ by up to 50 ka when comparing output from e.g. 50 ka and 200 ka filters, largely due to the presence of some orbital variability in the 50 ka filter (likely the 54 ka obliquity component). It is therefore important to emphasize here that the processing method, as well as the age model uncertainties, provides approximate timings of trends and should be considered with these uncertainties in mind. Temperature anomalies between different climate windows were also calculated using the mean SSTs for the "41 ka world" (1.3 – 1.5

Ma), the "100 ka world" (0 – 0.5 Ma) and two intervals during the intervening transition state (0.6 – 0.8 Ma and 0.9 – 1.1 Ma) (Table 2).

3.3.2 Trends in glacial and interglacial maxima

To evaluate the role of glacial and/or interglacial variability in driving the long-term SST trends, we examined the patterns of glacial and interglacial SSTs across the last 2 Ma (see Herbert et al., 2010, for similar analysis)(Table 3). We also apply this approach to the LR04 benthic $\delta^{18}O$ stack (Lisiecki and Raymo, 2005), ice core pCO_2 record (Luthi et al., 2008), and Fe-mass accumulation record of dust inputs to the Subantarctic Atlantic (Martinez-Garcia et al., 2011). We define glacial and interglacial maxima across the last 2 Ma from the benthic oxygen isotope record ($\delta^{18}O_b$) used to create the age model for each site (Table 1). SST maxima were picked within a 10-ka window around the interglacial or glacial peak, to allow for uncertainty associated with identifying the interglacial or glacial maxima for each site, the tuning approach, and to account for changes in the length and structure of interglacial periods (Tzedakis et al. 2009). Records with a sampling resolution exceeding 5 ka were not used in our analysis because they do not adequately resolve interglacial or glacial peaks within the 10 ka window, and continuous records were chosen in order to depict the long-term Pleistocene trend.

3.3.2 Wavelet analysis

To determine the evolution of periodic variability in the SST records, orbitally-calibrated records were analyzed by a continuous wavelet transform method (Grinsted et al., 2004). This particular method includes a test for statistically significant wavelet power against background red noise, as well as identifying areas of the spectra where edge effects might affect the results (the "cone of influence"). Using the WTC-16 Matlab code (Grinsted et al., 2004) all data sets were first linearly interpolated to the average sample spacing of each record (2.0-6.5 ka). As a result, periodicities relating to precession likely lie close to the limits of detection with this method.

4. RESULTS

4.1 Trends in mean SSTs

To determine whether there is a consistent pattern in the timing of secular SST change during the Pleistocene we focus here on the long-term trends at each site i.e. those upon which glacial-interglacial and higher frequency variability is superimposed. A complex set of long-term trends is produced following application of a 200 ka bandpass filter (Figure 2). The SiZer analysis determines which of these trends is significant (statistically different to a zero gradient) and at which bandwidth. We focus here on trends which are significant at bandwidths of 200 ka and longer, although shorter term variability can be seen in the SiZer maps (Figure 3).

Figures 2 and 3 identify three general patterns of SST change over the last 2 Ma: (1) almost all of the records (21 out of 27) are characterized by a long-term cooling trend prior to ~0.8 Ma (Figure 2, Table 2). This is especially pronounced in the upwelling systems of Benguela (~3.8-4.7°C), Peru and California (~2.0-2.8°C). High-

latitude, non-upwelling sites cool by ~2.0-2.5°C (NW Pacific, northern N Atlantic) and ~1.6-2.0°C (Subantarctic Atlantic, east equatorial Pacific; Table 2). The timing of the onset of cooling varies among sites but generally occurs in the interval between 1.6 and 1.3 Ma. From 1.2 Ma there is an intensification of cooling (Figures 2 and 3). Between 0.9-0.6 Ma the cooling trend ceases in most sites, with no discernible trend toward the present; (2) In several locations, in particular for the equatorial Atlantic (662), NW Pacific (882), SE Atlantic (1087), Subantarctic Atlantic (1090), SW Pacific (1123), and the Coral Sea (MD06-3018), the mid- and late-Pleistocene is marked by long-term warming (Figures 2 and 3); and (3) Sites from the western Pacific warm pool (WPWP) show no clear long-term SST trend. Although a long-term (>250 ka) cooling is shown at one WPWP site, MD97-2140 (Figure 3), the magnitude of the SST change across the complete record is less than 1°C, and thus well within the uncertainties of the temperature calibrations. As a result, we consider that there is no statistically significant trend in WPWP SSTs over the last 2 Ma.

4.2 Trends in glacial and interglacial maxima

To understand the factors controlling the long-term trends in mean SST, we assess whether the cooling trends are driven by either glacial and/or interglacial temperature change. Indeed, contrasting histories of SST change are revealed through comparisons of glacial and interglacial maxima. Interglacial SST trends from the high northern and mid southern latitudes (sites 982, 1123, 1090; $R<0.4$) show no discernible long-term change across the Pleistocene whereas SST trends from the mid northern latitudes (sites 607, 1020) show a slight cooling ($R>0.4$; Table 3; Figure 4b). At tropical

latitude sites (sites 722, 1146, 806, 1012, MD97-2140) there is no shift toward cooler or warmer interglacial temperatures (Figure 4a) except at the Coral Sea site (MD06-3018, Table 3) which warms over the last 2 Ma. Overall, there is either no mean interglacial cooling or a slight cooling in some sites from the high latitudes (<2°C over 2 Ma). Lang & Wolff (2011) evaluated SST interglacial maxima across the last 9 terminations and showed an obvious step-like increase in SST maxima associated from pre- to post-MBE (~450 ka) interglacials at higher latitude sites and a relatively small increase in SST maxima at tropical sites. Our analysis shows these similar features but as our data sets include SSTs for the last 2 million years the MBE SST change no longer stands out, as post-MBE interglacial SSTs are comparable to those of the early Pleistocene (Figure 4b). Several records show that interglacial SSTs reached their minima during the 0.8-1.0 Ma interval. This is particularly pronounced in the high latitudes (Figure 4b) but can also be identified as an isolated cool interglacial at 0.908 Ma (MIS 23) in the tropical records (Figure 4a).

High northern latitude and mid-southern latitude glacial SSTs (sites 607, 982, 1090) exhibit a long term cooling (R=~0.4-0.7) trend of 3.0-6.0 °C over the last 2 Ma, but there is more variability between glacial maxima than in the interglacial records (Table 3; Figure 5). Pronounced cooling (i.e. deviation from the long term mean) occurs between 0.8-1.0 Ma in the north Atlantic (982) and subantarctic Atlantic (1090) sites (Figure 5b). In contrast, glacial SSTs at site 1123 (SW Pacific) show an overall increase through the Pleistocene. Sites from tropical latitudes show a diverging pattern (Figure 5a). All sites from upwelling regimes (846, 1012) show a decrease in glacial SSTs across the Pleistocene, as do sites 722 and 1146 (Indian Ocean, South China Sea). Pronounced glacial cooling between 0.8 and 1.0 Ma is also observed at these sites,

although this is confined to MIS 22-24 (~0.9 Ma) at sites 722 and 1146. In contrast, sites from the western equatorial Pacific warm pool show no trend over the last 2 Ma (Figure 5a). Overall, high latitudes, mid-latitudes, and upwelling regimes show a consistent shift toward cooler glacial SSTs across the Pleistocene.

4.3 Evolution of orbital-scale variability

The MPT is clearly defined in the $\delta^{18}O_b$ record as a shift in dominant period from ~41 ka to quasi-100 ka (Imbrie et al., 1993; Mudelsee and Schulz, 1997). In the LR04 $\delta^{18}O_b$ stack, statistically significant ~100 ka cycles emerge from 0.9 Ma (Figure 6). A more complex expression of evolving periodicities is revealed by the individual SST records (Figure 6). Strong 41 ka cycles are evident but intermittent in almost all records prior to 0.8 Ma. The shift to 100 ka cycles is most clearly expressed in the east Pacific cold tongue (846), the Coral Sea (MD06-3018), Benguela upwelling (1082), and the Subantarctic Atlantic (1090) sites. The earliest onset of statistically significant quasi-100 ka cycles in SST records occurs at ~0.7 Ma (sites 846, 1082) and in the $\%C_{37:4}$ record in subantarctic Atlantic site 1090. However, the 100 ka cycles may be emerging as early as 1.2 Ma (e.g. sites 607, 846, 1020). There is no abrupt shift from one dominant period to the other in the SST records examined here.

5. DISCUSSION

Our analysis of new and pre-existing SST records spanning the last 2 Ma reveals several important new insights. Most sites exhibit an overall cooling trend across the

early Pleistocene which intensifies between 1.2 and 0.8 Ma. However, six sites display warming trends that span the mid and/or late Pleistocene (sites 662, 882, 1087, 1090, 1123, GIK, MD06-3018). Three of these records (1123, GIK, MD06-3018) showed no cooling trend, nor did they span the whole 2 Ma study interval to set the late Pleistocene warming into context. Furthermore, although SiZer analysis considers the Coral Sea warming to be statistically significant at the >200 ka bandwidth (Figure 3), the original authors consider this trend to be insignificant since at <0.5°C it occurs within the uncertainty range for the Mg/Ca-SST calibration (Russon et al., 2010). In the WPWP there is no significant trend in mean SSTs.

When comparing glacial and interglacial maxima, we have shown that there is no long-term trend in interglacial SST across the Pleistocene at most sites. In contrast, at high latitudes, upwelling regions, in the Indian Ocean and northern South China Sea, glacial temperatures cool through the Pleistocene. Between 0.8 and 1.0 Ma most sites show pronounced cooling of both glacials and interglacials, except in the WPWP where there is little discernible change in glacial or interglacial maxima over the last 2 Ma. As observed for the long-term SST means, a few sites show evidence for intermittently warmer glacial maxima after the MPT; thus, the 100 ka cycles are not necessarily characterized by the coldest glacial SSTs of the Pleistocene in all regions.

A shift from 41 ka to 100 ka periodicities at 0.8 Ma can be identified in many of the SST records, although it tends to be gradually expressed and may involve emergence of 100 ka periodicity as early as 1.2 Ma, before it becomes statistically significant. The evidence thus far shows that the shift to 100 ka SST periodicity occurs later than the onset and intensification of long term trends in mean and glacial SSTs. Here, we consider the implications of these results for current hypotheses about the

mechanisms responsible for the MPT. First, we consider the relative impact of individual site records on the trends that we have observed.

5.1. Regional expressions of Pleistocene SST change

The majority of records show a long-term cooling trend through the early and mid-Pleistocene, but it is also clear that the timing of the onset of this cooling varies between sites (Figure 2). This is to be expected given contrasting regional sensitivities to e.g. frontal systems, thermocline depth, and wind intensity. The greatest intra-regional variability between long-term trends is found in the east equatorial Pacific upwelling sites, which cool by ~1.0 to 1.7°C during a broad time window stretching between 1.7 and 0.9 Ma (Figure 2). This variation may reflect the differing temporal resolution and thus potential sampling bias of site 847 (early cooling, 12-20 ka spacing, Mg/Ca-SSTs) compared to sites 846 and 849 (later cooling, 2-5 ka spacing, U^{K}_{37}'-SSTs) which are very similar in both their timing and magnitude of long-term SST change. In the California margin, long-term cooling begins in the northernmost site (1020, ~1.5 Ma) earlier than in those to the south (1014, 1012, from ~1.2-1.4 Ma), but this likely reflects the reduced influence of upwelling and enhanced sensitivity to high latitude circulation at site 1020.

The common pattern which unites most records presented here is one of early Pleistocene long-term cooling, which intensifies from 1.2 Ma and is marked by pronounced glacial and interglacial cooling around 0.9 Ma (MIS 22-24). The long-term cooling trends are then diminished or cease and the onset of 100 ka cycles begins from ~0.8 Ma. It is important to consider the processes which might control the SST

signatures discussed here, since these may give insight into the mechanisms which are responsible for both ocean circulation change and the ice-sheet growth associated with the MPT.

At all sites from the WPWP there is no discernible trend in mean, maximum or minimum SSTs through the interval of study (Figures 2-5). This temperature stability in the WPWP suggests that the overall cooling observed in the east Pacific upwelling sites represents a long-term intensification of the zonal SST gradient and thus the strengthening of Walker Circulation. Likewise, the overall cooling trends observed in the high latitudes of the Pacific lead to enhanced meridional SST gradients and thus overall intensification of Hadley Circulation through the Pleistocene. In line with these changes, long-term cooling is observed at sites 722 (Arabian Sea), 1143 and 1146 (southern and northern South China Sea), both located northward of the margins of the WPWP at the present day. The increasing SST gradient between the marginal and central WPWP sites as well as the increasing zonal SST gradient indicates a contraction of the western, eastern and northern margins of the WPWP through the Pleistocene. This pattern is consistent with strengthening Hadley and Walker Circulation (Jia et al., 2008; Li et al., 2011), indicative of the final stages of a long-term, gradual increase in zonal and meridional SST gradients (and associated circulation change) which began ~2 Ma and 3.5 Ma, respectively (Brierley and Fedorov, 2010). However, the stability of the Coral Sea SSTs (MD06-3018) through the Pleistocene suggests that the southern margin of the WPWP did not contract equatorward, and suggests that Hadley Circulation in the southern hemisphere was probably not strengthened in association with the MPT (Russon et al., 2010). Among the potential causes for this contrasting inter-hemispheric response in Hadley Circulation systems could be a difference in the magnitude of polar

cooling in the respective hemispheres (Jia et al., 2008). Alternatively, the complex hydrography of the Coral Sea means that the MD97-3018 site might also reflect changing current positions not just regional circulation change. We discuss the evidence for changing ocean/atmosphere circulation systems below, but note here that the Pacific Subantarctic site (1123) shows similarly atypical SST trends (warming) across the MPT to those observed in the Coral Sea.

5.1.1 Early (pre 1.2 Ma) cooling

The common cooling interval between 1.2 and 0.8 Ma represents an intensification of a longer-term cooling trend in several regions, specifically in high latitude and eastern boundary regions, including the Subantarctic Atlantic (site 1090), north Atlantic (site 607) and eastern boundary upwelling systems (Benguela, Peru, California). Cooling is also observed in the long-term trend of the Atlantic deep-water temperature (DWT-A, Figure 2) record (also 607) from ~1.5 Ma (Sosdian and Rosenthal, 2009). Cooling in the Pacific deep-water temperature record (DWT-P, Figure 2) (Elderfield et al., 2012) occurs before 1.3 Ma, but identifying the timing of the cooling onset is limited by the record only extending back to 1.5 Ma. The pattern of cooling in the long-term means is driven by declining SSTs during glacial maxima; no trend in interglacial SSTs is observed at this time (Figures 4 and 5). No shift in periodicity of the SST records occurs: they continue to be dominated at the 41 ka (obliquity) period through the early Pleistocene, slightly leading (< 5 ka) or in phase with benthic $\delta^{18}O$ in the tropical, north Atlantic and Subantarctic Atlantic (Herbert et al., 2010; Lawrence et al., 2011; Martinez-Garcia et al., 2010). The two records of deep-

water temperature also slightly lead (DWT-A) or are in phase (DWT-P) with $\delta^{18}O_b$ in the obliquity band (Elderfield et al., 2012; Sosdian and Rosenthal, 2009).

The overall cooling at Subantarctic Atlantic site 1090 (Martinez-Garcia et al., 2010; Rodríguez-Sanz et al., 2012) is accompanied by an increase in the concentration of the $C_{37:4}$ alkenone (Figure 3) and decreased local seawater $\delta^{18}O$, argued to reflect cooling and freshening of the surface ocean, and an equatorward expansion of polar water masses (Martinez-Garcia et al., 2010; Rodríguez-Sanz et al., 2012). This interpretation is supported by the presence of laminated diatom mats in the same region, which show a polar front ~6° equatorward of its modern location between 1.3 and 0.9 Ma (Kemp et al., 2010). The diatom mat record is incomplete prior to 1.3 Ma, which limits our ability to assess the timing of onset of this frontal displacement. However, planktonic foraminifera assemblages at site 1090 suggest that the polar front may have been displaced equatorward from as early as 1.8 Ma (Becquey and Gersonde, 2002). A long-term cooling trend is also observed at site 1087 (Figure 2), supporting the notion of an equatorward shift of the Antarctic Circumpolar Current (ACC); SSTs at site 1087 have been interpreted to reflect the position of the ACC via its impact on Agulhas Leakage to the SE Atlantic (McClymont et al., 2005). Similarly, contemporaneous high-latitude cooling and freshening in sub-Arctic NW Pacific surface waters is also suggested by increasing concentrations of the $C_{37:4}$ alkenone at site 882 (Martinez-Garcia et al., 2010).

Strengthening meridional SST gradients in response to polar cooling during early Pleistocene glacial stages could account for the concomitant cooling observed in the upwelling regimes via intensification of trade winds strength and upwelling. Enhanced dust inputs to the Subantarctic Atlantic from ~1.5 Ma (Martinez-Garcia et al.,

2011) are consistent with strengthening atmospheric circulation in the southern hemisphere, and increased organic matter accumulation in the Peru margin marks the development of a more productive upwelling regime (Dekens et al., 2007). Propagation of high latitude cooling to the upwelling regions might have occurred via the thermocline (Fedorov et al., 2006; Lee and Poulsen, 2006) and/or intermediate and deep water masses (Lawrence et al., 2011). Deep-water cooling in the deep north Atlantic (Sosdian and Rosenthal, 2009) and SW Pacific (Elderfield et al., 2012) prior to 1.3 Ma is concordant with changes in high latitude SST in both the northern and southern hemispheres, respectively. However, assessment of the relative contributions of atmospheric and/or ocean mechanisms for explaining the links between low and high latitude SST change through the early Pleistocene requires further development of archives recording the thermal structure of the ocean interior and changes to atmosphere and ocean circulation.

5.1.2 Accelerated cooling from 1.2 to 0.9 Ma and a "premature" 100 ka cycle

From 1.2 Ma, an intensification in the cooling trend in long term mean SSTs occurs at almost all sites (Figure 2), driven largely through continued cooling of glacial maxima (Figure 5) but accompanied by decreasing SSTs during interglacial maxima in the north Atlantic (Figure 4b) and upwelling regions (Figure 4a). The interglacial SST cooling seen in the North Atlantic is likely a consequence of reduced interglacial NADW formation after ~1.2 Ma and suppression of associated northward heat transport (Sexton and Barker, 2012). Expansion of polar waters during both glacials and interglacials occurred in the northern North Atlantic ($\%C_{37:4}$, McClymont et al., 2008)

accompanying the earlier (pre-1.2 Ma) polar water expansion in the NW Pacific and Southern Oceans (Martinez-Garcia et al., 2010). Trade winds (and/or aridity of source regions) intensified in the Atlantic at ~1.2 Ma, as recorded by increasing aeolian inputs and decreasing SSTs in the Canary Current region (Pflaumann et al., 1998) and off east and west equatorial Africa (de Menocal, 2004) (Figures 2-4), and enhanced inputs of terrigenous clays to the Southern Ocean (Diekmann and Kuhn, 2002). As seen prior to 1.2 Ma, this apparent strengthening of Hadley circulation is likely a response to the magnitude of cooling in the high latitudes exceeding that observed in the tropics, further intensifying the meridional SST gradient (Martinez-Garcia et al., 2010). Strengthening of the East Asian monsoon from 1.2 Ma is also consistent with intensification of Hadley circulation (Jia et al., 2008; Sun et al., 2006). In the absence of an SST trend in the WPWP, continued cooling of the east Pacific upwelling sites indicates further strengthening of zonal Pacific SST gradient and Walker Circulation from 1.2 to 0.9 Ma (McClymont and Rosell-Melé, 2005). SST minima are reached in the Subantarctic Atlantic site early in this time window, ~1.1-1.2 Ma (Figure 2; Martinez-Garcia et al., 2010; Rodríguez-Sanz et al., 2012), with relatively warmer glacial and interglacial stages and reduced $\%C_{37:4}$ values occurring after ~1.0 Ma (Figures 3 and 4) (but these are still, on average, below their early Pleistocene values). This intensified Southern Ocean cooling is consistent with the conclusion that ventilation in the Pacific sector of the Southern Ocean may have become more important for glacial abyssal circulation at ~1.1 Ma (Sexton and Barker, 2012) and explains a rapid switch in glacial-interglacial carbonate sedimentation cyclicity between the Pacific and Atlantic at this time (Sexton and Barker, 2012). The SW Pacific smoothed DWT record from site 1123 appears comparatively stable through the 1.2-0.9 Ma time window, having warmed from a

minimum at 1.3 Ma (Figure 2). This stability is perhaps surprising, given the very large SST changes seen at a site (1090; Martinez-Garcia et al., 2010) near the 'upstream' source region of the CDW that currently bathes Site 1123. The warming in DWT-P leads that of the SAA site (1090), revealing that different sectors of the Southern Ocean may have had different thermal histories, supporting the suggestion (Sexton and Barker, 2012) that the Pacific sector of the Southern Ocean may be particularly important for changing deep water circulation through the MPT. The high latitudes of the Pacific (site 882) are anti-correlated with the SAA SST trend (site 1090) between 1.2-0.8 Ma (Figure 2); whether this reflects a difference between Atlantic and Pacific high latitude climate evolution requires additional evidence from the Pacific sector of the Southern Ocean.

The intensification of cooling at 1.2 Ma is also marked by the presence of a "premature" 100 ka cycle in many records, corresponding to MIS 35-34 (Figure 7). The extended glacial-interglacial cycle at 1.2 Ma was first noted in the $\delta^{18}O_b$ record (Mudelsee and Stattegger, 1997). It has since been identified in carbonate sedimentation records from the Atlantic and Pacific (Schmieder et al., 2000), DWT from the SW Pacific (Elderfield et al., 2012) and is marked in the Chinese loess record as an unusually coarse loess unit ('L_{15}') suggesting that the strength of the Asian monsoon system was perturbed (Heslop et al., 2002; Sun et al., 2006). In many of the SST records examined here, as well as those from the Nordic Seas (Helmke et al., 2003), and the Canary Current (Pflaumann et al., 1998), MIS 35 is a time of pronounced and/or extended interglacial warmth. The presence of this "100 ka" cycle has been used to argue that the climate system was close to a threshold for a shift to late Pleistocene-style glaciations (Mudelsee and Stattegger, 1997), but that other feedbacks had yet to develop. In Figure 7 we show that a 100 ka cycle at ~1.2 Ma is present in SST records

globally, as well as in the LR04 stack and the deep-water temperature records from sites 607 (DWT-A) and 1123 (DWT-P). However, it is worth noting that, in contrast to the late Pleistocene 'saw-tooth' 100 ka cycles, MIS 35 is symmetric in form, with its onset phase marked by a gradual glacial termination (MIS 36), a subsequent prolonged interglacial (MIS 35), followed by a gradual return to glacial (MIS 34) conditions.

5.1.3 The "900 ka event"

The cooling trend that commenced ~1.2 Ma typically ceases or is reduced in intensity by ~0.8 Ma. This follows pronounced, but short-term, cooling during glacial and interglacial stages between 0.95 and 0.85 Ma (MIS 24-22) in almost every site that we examined (Figures 4 and 5, 7). Such a phenomenon was also identified by Clark et al. (2006) and Kemp et al. (2010) and termed "the 900 ka event". Here, we show that MIS 24-22 is marked by anomalously cool SSTs in most Pleistocene records (Figures 4,5,7). A pronounced glacial cooling is not evident in the WPWP sites (Figures 4,5), although an alkenone record from site 806 did identify MIS 24-22 as a time of sustained, relatively cold SSTs within the 0.5-1.5 Ma window (McClymont and Rosell-Melé, 2005). A cool interglacial during MIS 23 is, however, observed in the WPWP (Figure 4). That the perturbation to SSTs during MIS 24-22 might mark the crossing of some form of climate threshold is supported by the evidence for a number of climate shifts from this time. A southward displacement of the African monsoon system occurred after 0.95 Ma, accompanied by the development of sub-orbital scale variability (Larrasoaña et al., 2003). At 0.9 Ma, east Asian monsoon intensity weakens (Heslop et al., 2002), coincident with a stepped increase in the amplitude and period (to 100 ka) of

the Arabian monsoon (de Menocal, 2004) and a shift towards more C_4 vegetation in the Congo basin (Schefuß et al., 2003). These results are indicative of more arid conditions developing onshore from MIS 24-22 onwards, particularly in the tropical and subtropical regions.

MIS 24-22 is also marked by changes to deep water ventilation, but these tend to be sustained beyond the duration of the "900 ka event". The largest benthic $\delta^{13}C$ excursion of the last 5 million years occurred during MIS 24-22, and is argued to reflect an enhanced contribution of southern-sourced waters to the deep Atlantic from 0.9 Ma and/or decreased export of NADW (Elderfield et al., 2012; Raymo et al., 1997). Although the benthic $\delta^{13}C$ excursion is limited in duration, it marks the onset of enhanced carbonate dissolution (Schmieder et al., 2000) in the deep south Atlantic. An increased contribution of southern-sourced waters to the Atlantic (rather than changing north Atlantic ventilation patterns) during this interim state is further suggested by the stability of the vertical $\delta^{13}C$ profiles in the north Atlantic which span the broad window of 1.8 to 0.6 Ma (Raymo et al., 2004). However, there is also evidence for weaker deep water ventilation in the Atlantic sector of the Southern Ocean in response to more extensive glacial sea ice distributions after 0.9 Ma, but particularly pronounced during MIS 24-22 (Diekmann and Kuhn, 2002). As noted above, resolving the relative contribution of southern sourced waters to the deep ocean and its response to the surface ocean events described here, requires additional evidence beyond the Atlantic deep water source regions.

In addition to defining the end of the early Pleistocene cooling trend and a time of pronounced cooling, MIS 24-22 also marks the onset of dominant 100 ka cycles in

the benthic $\delta^{18}O$ stack (Figure 6). Statistically significant and dominant 100 ka cycles typically develop later in SST records, generally after 0.8 Ma (Figure 6). At site 1090, SST with 100 ka period leads benthic $\delta^{18}O$ by ~11 ka or half a precession cycle, from 0.7 Ma to present (Martinez-Garcia et al., 2010). Emergence of 100 ka periodicity in tropical SSTs also develops after 0.9 Ma, and is in phase with or leads (<5 ka) benthic $\delta^{18}O$ (Herbert et al., 2010). DWTs also lead benthic $\delta^{18}O$ after 0.85 Ma in the north Atlantic and SW Pacific (Elderfield et al., 2012; Sosdian and Rosenthal, 2009). In contrast, north Atlantic SSTs and benthic $\delta^{13}C$ oscillate in phase with, or slightly lag, benthic $\delta^{18}O$ (Lawrence et al., 2011) before and after the MPT.

5.1.4 The Mid-Brunhes Event in the context of 2 Ma of SST evolution

The shift towards warmer interglacial temperatures and higher pCO_2 concentrations in the Antarctic ice cores ~0.4 Ma, the MBE, was reviewed recently in terms of both marine and terrestrial evidence (Lang and Wolff, 2011; Masson-Delmotte et al., 2010). We therefore do not repeat the discussions here nor focus on the possible causes for such a warming trend. However, we note that in general the evidence for "unusual" interglacial warmth following the MBE is less clearly expressed when the 2 Ma SST history is presented. In most cases, the post-MBE interglacials return to early Pleistocene SST values (Figure 4). Instead, it is the MPT and pre-MBE time window that appears unusual from a broader Pleistocene perspective for containing relatively cool interglacials.

Several regions also show that the overall warming trend towards the present day after MIS 10 occurs in both interglacials and glacials (Figures 2-4). This is

particularly clearly expressed in SST records from the high latitudes of the southern hemisphere, especially those sites which are sensitive to ACC location, as well as in the Coral Sea. Consequently, mechanisms to invoke enhanced latest Pleistocene interglacial warmth as a response to the preceding intense glacial stages (Lang and Wolff, 2011) are difficult to reconcile with the evidence from SSTs, particularly when comparable interglacial warmth also occurred in the early Pleistocene with less intense glacial SST maxima. We assess the possibility of other forcing factors to explain early Pleistocene warmth below, and highlight here that "extreme" or "unusual" interglacial warmth following the MBE is less significant in the presence of 2 Ma SST trends and when evaluated at a global scale. The strong signal of post-MBE warming in regions which are sensitive to the position of the ACC might therefore be explained by long-term poleward retreat of the ACC fronts, following their prior, equatorward migration near the MPT (Kemp et al., 2010). Thus ,the post-MBE warming of interglacials may not have been a global phenomenon.

5.2 Implications for mechanisms to explain the MPT

We have presented a range of SST trends, with different regional expressions in terms of magnitudes and timings, but united by a shift toward a mean cooler surface ocean over the last 2 Ma, except in the WPWP. The prominent feature which occurs in almost all of the records is an intensification of a cooling trend from 1.2 Ma, driven largely through progressive decreases in the SSTs of glacial maxima, which ends with pronounced cooling across MIS 24-22 ~0.9 Ma.

Previous analyses of $\delta^{18}O_b$ (Mudelsee and Schulz, 1997) indicated that the timing of the MPT onset was 0.9 Ma, marking a rapid increase in continental ice volume. Recent reconstructions of seawater $\delta^{18}O$ in the SW Pacific support this pattern (Elderfield et al., 2012). An increase in ice volume was considered to be critical for developing ice-sheet inertia in response to orbital forcing, thus leading to the development of the quasi-100 ka cycles which dominated from 0.6 Ma (Mudelsee and Schulz, 1997). However, two features of the observed SST evolution suggest that SST cooling may have been either a necessary precursor to evolving ice-sheet dynamics or may, more generally, point to important mechanisms in the genesis of quasi-100 ka ice volume cycles. First, the onset of SST cooling from 1.2 Ma coincides with the development of a stable (but anti-correlated) relationship between $\delta^{18}O_b$ and eccentricity (Lisiecki, 2010), suggesting that the pacing of glacial cycles at the 100 ka period was linked with the timing of SST cooling identified here. Second, we have demonstrated that early emergence of 100 ka power occurs in several SST records at 1.2 Ma (Figure 6).

Seawater $\delta^{18}O$ reconstructions from the Atlantic versus Pacific give slightly different interpretations of the nature of MPT ice volume expansion. The Atlantic reconstruction calculated that a gradual glacial-age expansion of ice volume occurred between 0.9-0.6 Ma (Sosdian and Rosenthal, 2009). In contrast, a SW Pacific reconstruction reveals an abrupt increase in global ice volume at 0.9 Ma (Elderfield et al., 2012). Although subtle differences exist between the Atlantic and Pacific ice volume reconstructions across the MPT, both records are consistent in indicating no increase in glacial-age ice volume prior to 0.9 Ma, despite the evidence presented here for cooler glacials and cooler mean SSTs prior to this time (Figures 2-4). The ice-sheet

expansion associated with the MPT thus occurs after much of the surface ocean, as well as the deep Atlantic (Sosdian and Rosenthal, 2009), have already undergone long-term cooling from ~1.2 Ma. The increase in global ice volume at 0.9 Ma does, however, coincide with an interval of pronounced SST cooling spanning MIS 24-22.

A number of questions are raised by this relationship between SSTs and global ice volume. First, why did glacial stages experience progressive cooling in advance of ice-sheet growth? Second, is there any evidence for regional glaciation change which might be hidden within a globally integrated signal? Third, are the trends and patterns observed in the SST records mechanistically linked to the pattern of ice-sheet growth?

5.3.1 What drove SST cooling before 0.9 Ma?

One frequently invoked hypothesis to explain the MPT is that a progressive, long-term decline in atmospheric CO_2 caused climate and ice-sheets to cross a threshold (e.g. Berger and Jansen, 1994; Paillard, 1998). Under this scenario, a critical level of CO_2 was reached whereby ice-sheets were able to grow large enough to resist orbital forcing at the obliquity band, thus maintaining a critical mass during the next interval of higher solar insolation. With limited quantitative CO_2 data spanning the Pleistocene, most models simulate a long-term decline in CO_2 encompassing both glacial and interglacial stages (e.g. Paillard, 1998). None of the SST records examined here show a decline in interglacial SSTs prior to ice-sheet growth at 0.9 Ma, including sites from the WPWP which is expected to respond more to changes in radiative forcing rather than to continental ice-sheet feedbacks and regional ocean circulation change (Broccoli, 2000; Medina-Elizalde and Lea, 2005). This suggests that any CO_2-induced change in

radiative forcing was focused on the glacial stages between 1.2 and 0.9 Ma (Figure 5) but was not translated into the growth of larger glacial-age ice-sheets.

Atmospheric CO_2 is driven by a complex suite of processes and feedbacks, some of which can be examined using the data presented here. Between 1.5 and 1.0 Ma, the observed SST cooling of glacial stages records is accompanied by cooling of the abyssal Atlantic (Figure 2) (Sosdian and Rosenthal, 2009), elevated dust input to the Subantarctic Atlantic (Figure 5) (Diekmann and Kuhn, 2002; Martinez-Garcia et al., 2011), and more expansive subpolar water masses in the Subantarctic Atlantic followed shortly thereafter by the Pacific and north Atlantic (Martinez-Garcia et al., 2010; McClymont et al., 2008). The efficiency of the biological pump in the modern Southern Ocean is limited by the supply of micronutrients such as Fe (Sigman et al., 2010; Watson et al., 2000). Because elevated export production in the sub-Antarctic occurs in parallel with increased aeolian Fe supply during glacial maxima (Kumar et al., 1995; Kohfeld et al., 2006; Martinez-Garcia et al., 2009), iron fertilization via enhanced dust inputs to the Southern Ocean has been invoked to explain enhanced CO_2 drawdown during late Pleistocene glacial maxima (e.g. Kohfeld et al., 2005; Sigman et al., 2010). An exponential increase in Subantarctic dust accumulation began at 1.5 Ma, and intensified from 1.2 Ma (Martinez-Garcia et al., 2011). This dust has been confirmed as Fe-bearing illite clays from terrestrial sources, and is accompanied by increased glacial export production (Diekmann and Kuhn, 2002). This raises the possibility that intensification of the glacial dust/biological production/CO_2 feedback could account for some of the enhanced glacial SST cooling that we observe. The northward shift of the ACC that we described above could also have restricted the release of respired CO_2 from the deep ocean to the atmosphere, if accompanied by northward displacement of

the westerlies, more extensive sea ice cover and/or abyssal stratification (Sigman and Boyle, 2000; Toggweiler et al., 2006; Watson and Naveira Garabato, 2006). Abyssal storage of CO_2 may also have been enhanced by the freshening of the sub-Antarctic surface ocean (Rodríguez-Sanz et al., 2012). From 1.1 Ma, the onset of 'Pacific-style' $CaCO_3$ cycles (better preservation during glacials) in this, the largest and deepest ocean basin, may have enhanced alkalinity of the global ocean during glacials and contributed to glacial stage CO_2 drawdown (Sexton and Barker, 2012). These observations point to Southern Ocean hydrography, and its role in carbon cycling, in driving the pre-MPT (pre-0.9 Ma) glacial-stage SST cooling. However, to fully test this hypothesis requires higher resolution pCO_2 reconstructions for the early Pleistocene. In the absence of this detailed information, we now consider whether our SST compilation contains indirect evidence for changing pCO_2 prior to 0.9 Ma.

Although SST records reflect both global forcing and regional circulation patterns, the absence of any trend in interglacial temperatures pre-0.9 Ma suggests that either pCO_2 did not change, or that the sensitivity of the surface ocean to such forcing was damped. In comparing tropical SSTs through the Pliocene and Pleistocene, Herbert et al. (2010) demonstrated that not only were the records strongly unified in the timing and magnitude of the observed orbital and longer term variability, but that this unity could not be explained by direct solar radiation forcing of the tropics given the anti-correlation between SSTs and the predicted tropical forcing via obliquity and precession. They argued that this demonstrated the need for an underlying, common forcing mechanism to explain these patterns, and proposed that global radiative forcing via atmospheric CO_2 could be the cause. The resulting stacked SST record for the tropics shows evidence for gradual cooling from 1.5 Ma during both glacials and

interglacials (Herbert et al., 2010), consistent with a long-term decline in CO_2. However, the original SST records contained within that stack show that the cooling from 1.5 Ma is restricted to glacials (Figure 5), and the absence of any interglacial or glacial cooling trend in the centre of the WPWP (Figure 4, 5) does not support a long term CO_2 decline. Furthermore, in section 5.1 we outlined the possibility that the cooling SSTs in two of the four records comprising the tropical stack (Herbert et al., 2010) might instead reflect contraction of the WPWP, driven by strengthened Hadley and Walker circulation.

An alternative to CO_2 forcing is that strengthening of zonal and meridional SST gradients may have been an important prerequisite for the expansion of ice sheets at the MPT. Both snowpack formation and survival are enhanced by a strengthening of the meridional SST gradient by reducing the number of positive degree days and increasing snowfall below 70°N (Brierley and Fedorov, 2010). Increased zonal SST gradients in the equatorial Pacific appear to precipitate a weaker response in ice volume: a reduction in positive degree days occurs in the likely source regions of the Laurentide ice-sheet and increased snowfall ensues in Alaska and Greenland (Brierley and Fedorov, 2010). Furthermore, there is a direct impact on greenhouse forcing via changing water vapour and cloud formation. Figure 2 shows that the eastern and North Pacific cooled in tandem during the early and mid-Pleistocene. However, the WPWP did not cool, resulting in stronger zonal and meridional SST gradients (de Garidel-Thoron et al., 2005; Jia et al., 2008; Li et al., 2011; McClymont and Rosell-Melé, 2005; Medina-Elizalde and Lea, 2005) that potentially set the stage for Laurentide and Greenland ice-sheet growth (Brierley and Fedorov, 2010). Furthermore, the model simulations which invoke these relationships did not incorporate high latitude SST decline, which we

observe here, and which was noted (Brierley and Fedorov, 2010) would amplify ice sheet expansion. Although the model has its limitations, given that it does not include interactive ice-sheets and other forcings (Brierley and Fedorov, 2010), and meridional SST gradients in the southern hemisphere apparently did not intensify in the early Pleistocene (Russon et al., 2010), our findings (Figure 2) show that the evolving SSTs were likely preconditioning high northern latitudes for ice-sheet growth before the onset of the MPT.

5.3.2 When did continental ice sheets expand?

It has been argued that the fall in sea level during MIS 24-22 (and the origin of the MPT) reflects growth in the northern hemisphere ice-sheets (e.g. Berger and Jansen, 1994; Clark et al., 2006). An Antarctic contribution to increased global ice volume through MIS 24-22 has been suggested by the increase in seawater $\delta^{18}O$ in the SW Pacific (Elderfield et al., 2012) and a model of the West Antarctic ice-sheet (Pollard and DeConto, 2009). However, there are a number of indications of earlier ice-sheet advances in both hemispheres that might indicate regional ice sheet responses to changing SSTs and associated ocean circulation. An expansion of glaciers along the West Antarctic peninsula is suggested by enhanced deposition of ice-rafted debris from 1.35 Ma (Cowan et al., 2008), and it has been argued that the East Antarctic ice-sheet had grown to develop marine-based margins by ~1 Ma (Raymo et al., 2006). The northward displacement of the ACC during the early Pleistocene is consistent with ice sheet expansion since modeling studies predict positive feedbacks between growth of land ice and sea-ice (DeConto et al., 2007). The maximum extent of the Patagonian ice-

sheet has been dated to 1.1 Ma (Singer et al., 2004), coincident with our interpreted timing of ACC migration, and again also consistent with a northward displacement of the ACC and associated westerlies, as observed during the last glacial maximum (e.g. Hulton et al., 1994).

Evidence also exists for early ice-sheet expansions in the northern hemisphere before MIS 24-22. After 1.5 Ma the ice-sheet in the SW Barents Sea first reached the shelf edge (Solheim et al., 1998), and an advance of the Scandinavian ice-sheet into the northern North Sea Basin occurred ~1.1 Ma (Sejrup et al., 2000). Increased ice-rafting from the British and Irish ice-sheet developed from 1.2 Ma (Thierens et al., 2012). Enhanced ice-rafting to the Nordic Seas and north Atlantic resumes after 1.0 Ma (Fronval and Jansen, 1996; Ruddiman et al., 1986), and after 0.9 Ma from the Alaskan and Greenland ice-sheets (Sancetta and Silvestri, 1986). Thus, early Pleistocene ice-sheet advance by the northern hemisphere ice sheets is followed by some delay until repeated and extensive glaciations characterize the later Pleistocene. Transient and unusually large glacial-stage excursions to higher seawater $\delta^{18}O$ (e.g. higher global ice volume) before 0.9 Ma (e.g. MIS 32 and 34 ~1.1 Ma, and MIS 38 ~1.3 Ma) (Elderfield et al., 2012) appear to support these patterns of regional ice sheet advance.

These early ice-sheet advances coincide, within their dating errors, with both the onset/intensification of cooling in the SST records and the presence of the "premature" 100 ka cycle at 1.2 Ma. Thus, some of the climate conditions required for an extended glacial/interglacial cycle were already in place during MIS 35-34. Specifically, feedbacks were active that allowed the climate system response to "skip" an obliquity cycle. It is not clear what makes MIS 35-34 special in terms of the SST, DWT and $\delta^{18}O_b$ response to orbital forcing (Figure 7): the 100 ka cycle spans an interval of

relatively low eccentricity, but MIS 35 is maintained as an anomalously long interglacial. Because this event is characterized by a long interglacial and a symmetric warming/cooling cycle, rather than by a 'saw-toothed' intensification of glacial conditions (Figure 7), the 100 ka cycle spanning MIS 34-36 (1.2 Ma) may have resulted from different climate feedbacks or sensitivity to orbital forcing compared with those of the late Pleistocene ~100 ka cycles.

5.3.3 What delayed the sustained ice-sheet expansion until 0.9 Ma?

Although we have presented evidence for SST cooling and circulation change that would have been conducive to ice-sheet growth as early as 1.2 Ma, sustained expansion of global ice volume occurred somewhat later, during MIS 24-22 ~0.9 Ma. A number of processes might explain this delay.

If the MPT (0.9 Ma) is a function of changes in northern hemisphere ice sheet geometry in response to a changing basal substrate (Clark et al., 2006; Clark and Pollard, 1998), enabling thicker ice masses to develop with greater inertia and longevity in the face of modest insolation increases, the timing of ice-sheet expansion and development of the 100 ka cycles may be somewhat divorced from broader changes in global climate. Geochemical analysis of glacial sediments from the Laurentide ice-sheet support a transition from erosion of heavily weathered substrate towards crystalline bedrock beneath the ice-sheet through the Pleistocene (see review by Clark et al., 2006). Although it is clear from the SST records examined here that climate was evolving towards a state where larger ice-sheets were likely to be supported, a seawater $\delta^{18}O$ record reveals relatively stable global ice volume until an abrupt expansion occurs at

MIS 22 (Elderfield et al., 2012), suggesting that a more rapid series of events or feedbacks drove ice sheet expansion at 0.9 Ma. Thus, accounting for the delayed ice-sheet response to the SST trends observed here is an important factor in explaining climate evolution across the MPT.

Earth's orbital configuration between 1.1 and 0.9 Ma may have been crucial in inhibiting the establishment of ~100 ka glacial cycles. During this 200 ka interval the amplitude of eccentricity (and precession) forcing increased, leading to high amplitude variability in insolation forcing in the high latitudes in both hemispheres (Figure 7). This includes a large peak in northern hemisphere (65°N) summer insolation which is closely aligned with MIS 31 and is driven by coincident high eccentricity and obliquity (Figure 7). Evidence for unusual interglacial warmth during MIS 31 is found in the Nordic Seas (Helmke et al., 2003), northern north Atlantic (McClymont et al., 2008), the Antarctic margins (Scherer et al., 2008) and in the deep SW Pacific (Elderfield et al., 2012). Model simulations of the West Antarctic ice sheet show that a collapse during MIS 31 was particularly sensitive to the strong austral summer insolation (Pollard and DeConto, 2009). Thus, orbital forcing between 1.1 and 0.9 Ma may have inhibited ice-sheet growth following MIS 34, because the increase in amplitude of eccentricity (and precession) likely damped the slow feedbacks necessary for prolonged ice-sheet growth (2010), ultimately preventing the establishment of ~100 ka glacial cycles.

Another mechanism to delay ice sheet expansion until 0.9 Ma may lie with the equatorward migration of polar water masses and high latitude cooling and freshening between 1.2 and 0.9 Ma seen in the north Atlantic, NW Pacific and sub-Antarctic (Martinez-Garcia et al., 2010; McClymont et al., 2008). These high latitude

hydrographic changes may have caused a temporary, but negative, feedback to ice-sheet growth (McClymont et al., 2008) via the negative impact on water vapour transport to ice-sheet source regions from the more extensive sea ice cover expected to have been associated with the polar water mass expansion. Subsequent poleward retreat of polar water masses at 0.9 Ma (McClymont et al., 2008) then reduced the constraints over moisture supply and encouraged ice-sheet growth. Testing this hypothesis awaits further development and application of sea ice proxies.

The notion that the global carbon cycle may have changed in association with the "900 ka event" and the transition to 100 ka cycles finds support in the fall in pCO_2 during both glacials and interglacials from ~0.9 Ma (Hönisch et al., 2009). Although interglacial CO_2 concentrations subsequently rise in association with the MBE, late Pleistocene glacial pCO_2 concentrations are reached and sustained from ~0.9 Ma. Even though the decline in glacial-stage pCO_2 was relatively minor (~30 ppmv), it could still have been sufficient to enhance climate sensitivity to CO_2, especially when ice albedo feedbacks are taken into account (Van de Wal and Bintanja, 2009). These relationships may indicate the need for a set of critical thresholds in global temperature, sea ice extent, SST gradients and pCO_2 to all be crossed to enable the development of larger ice-sheets in the northern hemisphere and an evolving sensitivity to orbital forcing after 1 Ma.

To fully test the mechanisms which are responsible for driving the premature 100 ka cycle, the cooling to 0.9 Ma, the MIS 24-22 event and the subsequent evolution of the 100 ka cycles requires renewed focus on generating spatially distributed and high resolution archives of SSTs and associated proxies for ocean circulation change. Much of the data discussed here are focused on sites that are strongly affected by upwelling or

shifts in the positions of oceanographic fronts. Whilst this information is extremely valuable for the identification of sensitive shifts in climate, it becomes difficult to assess the relative contribution of local and regional factors in driving the observed trends. To fully assess what makes the premature 100 ka cycle and the 900 ka event different to the earlier 41 ka cycles requires the generation of highly resolved records of ocean circulation and a better understanding of the ocean's interaction with ice sheets and atmospheric circulation.

6 CONCLUSIONS

We have reviewed, re-analyzed and compared published records of sea-surface temperatures (SSTs) to assess the global and regional signals of the MPT in the surface ocean. In response to our research questions (section 1):

(1) *Do globally distributed SST records display a common cooling trend across the MPT?* Yes. Although some regional variability exists in the timing and magnitude of cooling during the early Pleistocene, nearly all locations cool between 1.2 and 0.8 Ma, indicating that the MPT is a globally distributed cooling event;

(2) *Did SSTs change gradually or abruptly?* Gradually. Trends span >200 ka through the early Pleistocene (from as early as 1.8 Ma). Cooling intensifies after 1.2 Ma, and is pronounced during both glacial and interglacial stages ~0.9 Ma (MIS 24-22);

(3) *Did global SSTs change synchronously or do regional overprints exist?* Both. The cooling from 1.2 Ma is largely globally synchronous, as is the pronounced cooling at 0.9 Ma. However, some oceanographic regimes show evidence for earlier change, including equatorward migration of polar waters and upwelling intensification, alongside evidence for strengthening atmospheric circulation and cooling of the deep ocean.

(4) *Did glacial-interglacial SST cycles become more intense across the MPT?* Generally, the glacial stages became more intense. For some sites, the glacials after the MPT are the coolest of the past 2 Ma. However, for many sites, and particularly those of the southern hemisphere, the glacial stages of the past 0.9 Ma are warmer than those of the mid and early Pleistocene.

(5) *did a shift in the period of glacial-interglacial cycles occur?* Yes. There is a shift towards dominant 100 ka cyclicity in the SST records examined here by 0.8 Ma, but this occurs gradually. Cycles with a 100 ka period start to emerge in several sites as early as 1.2 Ma.

The strongest expression of Pleistocene cooling in the surface ocean is found during glacial intervals; interglacials show minor or negligible temperature trends. We argue that this pattern reflects changes in the climatic feedbacks operating during glacials, via intensified atmospheric circulation, changing patterns of Southern Ocean deep water ventilation and/or dust feedbacks on export production. In turn, these may have driven a subtle lowering of glacial pCO_2. Cooling of upwelling systems and the mid- and high latitude oceans leads to intensification of both meridional and zonal SST gradients given the absence of any change in SSTs for the West Pacific Warm Pool.

In combination, we argue that these processes led to the development of larger ice-sheets and modified ice-sheet and climate response to regular orbital forcing. Potential causes for a delayed ice-sheet response (at 0.9 Ma) to the onset of cooling intensification (from 1.2 Ma) include evolution of the basal substrates of the northern hemisphere ice-sheets (Clark et al., 2006), unfavourable orbital forcing, temporary restrictions to ice sheet moisture supply by the high latitude oceans, and a possible threshold decline in glacial-stage atmospheric CO_2 concentrations at 0.9 Ma.

Acknowledgments

We acknowledge the financial support provided by Newcastle University HaSS Faculty Research Fund (to E.L.M.), a US-UK Fulbright Fellowship (to S.M.S.), and a Marie Curie International Outgoing Fellowship (235626, to A.R.M.). This research used samples and data provided by the Integrated Ocean Drilling Program (IODP). IODP is sponsored by the US National Science Foundation (NSF) and participating countries under management of Joint Oceanographic Institutions (JOI), Inc. We thank Zhonghui Liu and Ben Petrick for sharing unpublished data, and thank Phil Sexton, Aurora Elmore, Babette Hoogakker, Ian Candy, Stewart Jamieson, Ben Petrick, Alfredo Martinez-Garcia, and Alan Haywood for discussions and constructive comments.

References

Anand, P., Elderfield, H., 2003. Calibration of Mg/Ca thermometry in planktonic foraminifera from a sediment trap time series. Paleoceanography 18, 1050, doi:1010.1029/2002PA000846.

Anand, P., Elderfield, H., Conte, M.H., 2003. Calibration of Mg/Ca thermometry in planktonic foraminifera from a sediment trap time-series. Paleoceanography 18, 15, doi:10.1029/2002PA000846.

Barker, S., Cacho, I., Benway, H., Tachikawa, K., 2005. Planktonic foraminiferal Mg/Ca as a proxy for past oceanic temperatures: a methodological overview and data compilation for the Last Glacial Maximum. Quaternary Science Reviews 24, 821-834.

Bartoli, G., Hönisch, B., Zeebe, R.E., 2011. Atmospheric CO_2 decline during the Pliocene intensification of Northern Hemisphere glaciations. Paleoceanography 26, PA4213.

Becquey, S., Gersonde, R., 2002. Past hydrographic and climatic changes in the Subantarctic Zone of the South Atlantic – The Pleistocene record from ODP Site 1090. Palaeogeography, Palaeoclimatology, Palaeoecology 182, 221-239.

Bendle, J., Rosell-Melé, A., 2004. Distributions of U^{K}_{37} and U^{K}_{37}' in the surface waters and sediments of the Nordic Seas: Implications for paleoceanography. Geochemistry Geophysics Geosystems 5, Q11013, doi:11010.11029/12004GC000741.

Berger, A., Loutre, M.F., 1991. Insolation values for the climate of the last 10 Million years. Quaternary Science Reviews 10, 297-317.

Berger, W.H., Jansen, E., 1994. Mid-Pleistocene Climate Shift- The Nansen Connection, In: Johannessen, O.M., Muench, R.D., Overland, J.E. (Eds.), The Polar Oceans and Their Role in Shaping the Global Environment. Geophysical Monograph Series 84. American Geophysical Union, pp. 295-311.

Brassell, S.C., Eglinton, G., Marlowe, I.T., Pflaumann, U., Sarnthein, M., 1986. Molecular stratigraphy: a new tool for climatic assessment. 320, 129-133.

Brierley, C.M., Fedorov, A.V., 2010. Relative importance of meridional and zonal sea surface temperature gradients for the onset of the ice ages and Pliocene-Pleistocene climate evolution. Paleoceanography 25, PA2214.

Broccoli, A.J., 2000. Tropical Cooling at the Last Glacial Maximum: An Atmosphere–Mixed Layer Ocean Model Simulation. Journal of Climate 13, 951-976.

Brown, S.J., Elderfield, H., 1996. Variations in Mg/Ca and Sr/Ca ratios of planktonic foraminifera caused by postdepositional dissolution: evidence of shallow Mg-dependent dissolution. Paleoceanography 11, 543-551.

Candy, I., Coope, G.R., Lee, J.R., Parfitt, S.A., Preece, R.C., Rose, J., Schreve, D.C., 2010. Pronounced warmth during early Middle Pleistocene interglacials: Investigating the Mid-Brunhes Event in the British terrestrial sequence. Earth-Science Reviews 103, 183-196.

Chaudhuri, P., Marron, J.S., 1999. SiZer for Exploration of Structures in Curves. Journal of the American Statistical Association 94, 807-823.

Clark, P.U., Archer, D., Pollard, D., Blum, J.D., Rial, J.A., Brovkin, V., Mix, A.C., Pisias, N.G., Roy, M., 2006. The Middle Pleistocene Transition: Characteristics, Mechanisms, and Implications for Long-Term

Changes in Atmospheric pCO_2. Quaternary Science Reviews 25, 3150-3184, doi:3110.1016/j.quascirev.2006.3107.3008.

Clark, P.U., Pollard, D., 1998. Origin of the middle Pleistocene transition by ice sheet erosion of regolith. Paleoceanography 13, 1-9.

Conte, M.H., Eglinton, G., Madureira, L.A.S., 1992. Long-chain alkenones and alkyl alkenoates as palaeotemperature indicators: their production, flux and early sedimentary diagenesis in the Eastern North Atlantic. Organic Geochemistry 19, 287-298.

Conte, M.H., Sicre, M.-A., Rühlemann, C., Weber, J.C., Schulte, S., Schulz-Bull, D., Blanz, T., 2006. Global temperature calibration of the alkenone unsaturation index (U^{K}_{37}') in surface waters and comparison with surface sediments. Geochemistry Geophysics Geosystems 7, Q02005, doi:02010.01029/02005GC001054.

Conte, M.H., Thompson, A., Eglinton, G., Green, J.C., 1995. Lipid biomarker diversity in the coccolithophorid *Emiliania huxleyi* (Prymnesiophyceae) and the related species *Gephyrocapsa oceanica*. Journal of Phycology 31, 272-282.

Cowan, E.A., Hillenbrand, C.-D., Hassler, L.E., Ake, M.T., 2008. Coarse-grained terrigenous sediment deposition on continental rise drifts: A record of Plio-Pleistocene glaciation on the Antarctic Peninsula. Palaeogeography, Palaeoclimatology, Palaeoecology 265, 275-291.

Crowley, T.J., Hyde, W.T., 2008. Transient nature of late Pleistocene climate variability. Nature 456, 226-230.

Crundwell, M., Scott, G., Naish, T., Carter, L., 2008. Glacial-interglacial ocean climate variability from planktonic foraminifera during the Mid-Pleistocene transition in the temperate Southwest Pacific, ODP Site 1123. Palaeogeography, Palaeoclimatology, Palaeoecology 260, 202-229.

de Garidel-Thoron, T., Rosenthal, Y., Bassinot, F., Beaufort, L., 2005. Stable sea surface temperatures in the western Pacific warm pool over the past 1.75 million years. Nature 433, 293-297.

de Menocal, P.B., 1995. Plio-Pleistocene African climate. Science 270, 53-59.

de Menocal, P.B., 2004. African climate change and faunal evolution during the Pliocene-Pleistocene. Earth and Planetary Science Letters 220, 3-24.

DeConto, R., Pollard, D., Harwood, D.M., 2007. Sea ice feedback and Cenozoic evolution of Antarctic climate and ice sheets. Paleoceanography 22, PA3214, doi:3210.1029/2006PA001350.

Dekens, P., Ravelo, A.C., McCarthy, M.D., Edwards, C.A., 2008. A 5 million year comparison of Mg/Ca and alkenone paleo-thermometers. Geochemistry Geophysics Geosystems 9, Q10001, doi:10010.11029/12007GC001931.

Dekens, P.S., Lea, D.W., Pak, D.K., Spero, H.J., 2002. Core top calibration of Mg/Ca in tropical foraminifera: Refining paleotemperature estimation. Geochemistry Geophysics Geosystems 3, 1022, doi:1010.1029/2001GC000200. .

Dekens, P.S., Ravelo, A.C., McCarthy, M.D., 2007. Warm upwelling regions in the Pliocene warm period. Paleoceanography 22, PA3211, doi:3210.1029/2006PA001394.

Diekmann, B., Kuhn, G., 2002. Sedimentary record of the mid-Pleistocene climate transition in the southeastern South Atlantic (ODP Site 1090). Palaeogeography, Palaeoclimatology, Palaeoecology 182, 241-258.

Durham, E.L., Maslin, M.A., Platzman, E., Rosell-Melé, A., Marlow, J.R., Leng, M., Lowry, D., Burns, S.J., Party, a.t.O.L.S.S., 2001. Reconstructing the climatic history of the western coast of Africa over the past 1.5 m.y.: a comparison of proxy records from the Congo Basin and the Walvis Ridge and the search for the Mid-Pleistocene Revolution, In: Wefer, G., Berger, W.H., Richter, C. (Eds.), Proceedings of the Ocean Drilling Program, Scientific Results, pp. 1-46 [Online].

Elderfield, H., Ferretti, P., Greaves, M., Crowhurst, S., McCave, I.N., Hodell, D., Piotrowski, A.M., 2012. Evolution of Ocean Temperature and Ice Volume Through the Mid-Pleistocene Climate Transition. Science 337, 704-709.

Etourneau, J., Martinez, P., Blanz, T., Schneider, R., 2009. Pliocene-Pleistocene variability of upwelling activity, productivity, and nutrient cycling in the Benguela region. Geology 37, 871-874.

Fantle, M.S., DePaolo, D.J., 2006. Sr isotopes and pore fluid chemistry in carbonate sediment of the Ontong Java Plateau: Calcite recrystallization rates and evidence for a rapid rise in seawater Mg over the last 10 million years. Geochimica et Cosmochimica Acta 70, 3883-3904.

Fedorov, A.V., Dekens, P.S., McCarthy, M., Ravelo, A.C., deMenocal, P.B., Barreiro, M., Pacanowski, R.C., Philander, S.G., 2006. The Pliocene Paradox (Mechanisms for a Permanent El Nino). Science 312, 1485-1489.

Fronval, T., Jansen, E., 1996. Late Neogene Paleoclimates and Paleoceanography in the Iceland-Norwegian Sea: Evidence from the Iceland and Vøring Plateaus, In: Thiede, J., Myhre, A.M., Firth, J.V., Johnson, G.L., Ruddiman, W.F. (Eds.), Proceedings of the Ocean Drilling Program, Scientific Results 151, pp. 455-468.

Grinsted, A., Moore, J.C., Jevrejeva, S., 2004. Application of the cross wavelet transform and wavelet coherence to geophysical time series. Nonlin. Processes Geophys. 11, 561-566.

Hayward, B.W., Kawagata, S., Grenfell, H.R., Sabaa, A.T., O'Neill, T., 2007. Last global extinction in the deep sea during the mid-Pleistocene climate transition. Paleoceanography 22, PA3103, doi:3110.1029/2007PA001424.

Head, M.J., Gibbard, P.L., 2005. Early-Middle Pleistocene Transitions: The Land-Ocean Evidence, Geological Society, London, Special Publications, vol. 247.

Helmke, J.P., Bauch, H.A., Erlenkeuser, H., 2003. Development of glacial and interglacial conditions in the Nordic seas between 1.5 and 0.35 Ma. Quaternary Science Reviews 22, 1717-1728.

Herbert, T.D., Peterson, L.C., Lawrence, K.T., Liu, Z., 2010. Tropical Ocean Temperatures Over the Past 3.5 Million Years. Science 328, 1530-1534.

Heslop, D., Dekkers, M.J., Langereis, C.G., 2002. Timing and structure of the mid-Pleistocene transition: records from the loess deposits of northern China. Palaeogeography, Palaeoclimatology, Palaeoecology 185, 133-143.

Hönisch, B., Hemming, N.G., Archer, D., Siddall, M., McManus, J.F., 2009. Atmospheric Carbon Dioxide Concentration Across the Mid-Pleistocene Transition. Science 324, 1551-1554.

Hoogakker, B.A.A., Rohling, E.J., Palmer, M.R., Tyrrell, T., Rothwell, R.G., 2006. Underlying causes for long-term global ocean $\delta^{13}C$ fluctuations over the last 1.20 Myr. Earth and Planetary Science Letters 248, 1-15.

Hulton, N., Sugden, D., Payne, A., Clapperton, C., 1994. Glacier Modeling and the Climate of Patagonia during the Last Glacial Maximum. Quaternary Research 42, 1-19.

Huybers, P., 2007. Glacial variability over the last two million years: an extended depth-derived agemodel, continuous obliquity pacing, and the Pleistocene progression. Quaternary Science Reviews 26, 37-55.

Imbrie, J., Berger, A., Boyle, E.A., Clemens, S.C., Duffy, A., Howard, W.R., Kukla, G., Kutzbach, J., Martinson, D.G., McIntyre, A., Mix, A.C., Molfino, B., Morley, J.J., Peterson, L.C., Pisias, N.G., Prell, W.L., Raymo, M.E., Shackleton, N.J., Toggweiler, J.R., 1993. On the structure and origin of major glacial cycles. Part 2. The 100,000-year cycle. Paleoceanography 8, 699-736.

Imbrie, J., Kipp, N., 1971. A new micropaleontological method for quantitative paleoclimatology, In: Turekian, K.K. (Ed.), The Late Cenozoic glacial ages. New Haven, Connecticut: Yale University Press, pp. 71-181.

Jia, G., Chen, F., Peng, P., 2008. Sea surface temperature differences between the western equatorial Pacific and northern South China Sea since the Pliocene and their paleoclimatic implications. Geophysical Research Letters 35, L18609, doi:18610.11029/12008GL034792.

Jian, Z., Wang, P., Chen, M.-P., Li, B., Zhao, Q., Bühring, C., Laj, C., Lin, H.-L., Pflaumann, U., Bian, Y., Wang, R., Cheng, X., 2000. Foraminiferal responses to major Pleistocene paleoceanographic changes in the southern South China Sea. Paleoceanography 15, 229-243.

Jian, Z., Zhao, Q., Cheng, X., Wang, J., Wang, P., Su, X., 2003. Plio-Pleistocene stable isotope and paleoceanographic changes in the northern South China Sea. Palaeogeography, Palaeoclimatology, Palaeoecology 193, 425-442.

Kawagata, S., Hayward, B.W., Grenfell, H.R., Sabaa, A., 2005. Mid-Pleistocene extinction of deep-sea foraminifera in the North Atlantic Gateway (ODP sites 980 and 982). Palaeogeography, Palaeoclimatology, Palaeoecology 221, 267-291.

Kemp, A.E.S., Grigorov, I., Pearce, R.B., Naveira Garabato, A.C., 2010. Migration of the Antarctic Polar Front through the mid-Pleistocene transition: evidence and climatic implications. Quaternary Science Reviews 29, 1993-2009.

Kohfeld, K.E., Quere, C.L., Harrison, S.P., Anderson, R.F., 2005. Role of Marine Biology in Glacial-Interglacial CO_2 Cycles. Science 308, 74-78.

Kucera, M., Weinelt, M., Kiefer, T., Pflaumann, U., Hayes, A., Weinelt, M., Chen, M.-T., Mix, A.C., Barrows, T.T., Cortijo, E., 2005. Reconstruction of sea-surface temperatures from assemblages of planktonic foraminifera: multi-technique approach based on geographically constrained calibration data sets and its application to glacial Atlantic and Pacific Oceans. Quaternary Science Reviews 24, 951-998.

Lang, N., Wolff, E.W., 2011. Interglacial and glacial variability from the last 800 ka in marine, ice and terrestrial archives. Climate of the Past, 7, 361-380, doi:310.5194/cp-5197-5361-5201.

Larrasoaña, J.C., Roberts, A.P., Rohling, E.J., Winklhofer, M., Wehausen, R., 2003. Three million years of monsoon variability over the northern Sahara. Climate Dynamics 21, 689-698.

Laskar, J., 1990. The chaotic motion of the solar system: A numerical estimate of the size of the chaotic zones. Icarus 88, 266-291.

Laskar, J., Robutel, P., Joutel, F., Gastineau, M., Correia, A.C.M., Levrard, B., 2004. A long-term numerical solution for the insolation quantities of the Earth. A&A 428, 261-285.

Lawrence, K.T., Herbert, T.D., Brown, C.M., Raymo, M.E., Haywood, A.M., 2009. High-amplitude variations in North Atlantic sea surface temperature during the early Pliocene warm period. Paleoceanography 24.

Lawrence, K.T., Liu, Z., Herbert, T.D., 2006. Evolution of the Eastern Tropical Pacific Through Plio-Pleistocene Glaciation. Science 312, 79-83.

Lawrence, K.T., Sosdian, S., White, H.E., Rosenthal, Y., 2011. North Atlantic climate evolution through the Plio-Pleistocene climate transitions. Earth and Planetary Science Letters 300, 329-342.

Lea, D.W., Mashiotta, T.A., Spero, H.J., 1999. Controls on magnesium and strontium uptake in planktonic foraminifera determined by live culturing. Geochimica Et Cosmochimica Acta 63, 2369-2379.

Lea, D.W., Pak, D.K., Spero, H.J., 2000. Climate Impact of Late Quaternary Equatorial Pacific Sea Surface Temperature Variations. Science 289, 1719-1724.

Lee, S.-Y., Poulsen, C.J., 2006. Sea ice control of Plio-Pleistocene tropical Pacific climate evolution. Earth and Planetary Science Letters 248, 238-247.

Li, L., Li, Q., Tian, J., Wang, P., Wang, H., Liu, Z., 2011. A 4-Ma record of thermal evolution in the tropical western Pacific and its implications on climate change. Earth and Planetary Science Letters 309, 10-20.

Lisiecki, L.E., 2010. Links between eccentricity forcing and the 100,000-year glacial cycle. Nature Geoscience 3, 349-352.

Lisiecki, L.E., Raymo, M.E., 2005. A Pliocene-Pleistocene stack of 57 globally distributed benthic d18O records. Paleoceanography 20, PA1003, doi:1010.1029/2004PA001071.

Liu, Z., Altabet, M.A., Herbert, T.D., 2005. Glacial-interglacial modulation of eastern tropical North Pacific denitrification over the last 1.8-Myr. Geophysical Research Letters 32, L23607, doi:23610.21029/22005GL024439.

Liu, Z., Herbert, T.D., 2004. High-latitude influence on the eastern equatorial Pacific climate in the early Pleistocene epoch. Nature 427, 720-723.

Luthi, D., Le Floch, M., Bereiter, B., Blunier, T., Barnola, J.-M., Siegenthaler, U., Raynaud, D., Jouzel, J., Fischer, H., Kawamura, K., Stocker, T.F., 2008. High-resolution carbon dioxide concentration record 650,000-800,000 years before present. Nature 453, 379-382.

Marlow, J.R., 2001. Application of U^{K}_{37}' for Long-term (Pliocene-Pleistocene) Palaeoclimate Reconstruction, Fossil Fules and Environmental Geochemistry. University of Newcastle upon Tyne, Newcastle upon Tyne.

Marlow, J.R., Lange, C.B., Wefer, G., Rosell-Melé, A., 2000. Upwelling intensification as part of the Pliocene-Pleistocene climate transition. Science 290, 2288-2291.

Marlowe, I.T., Brassell, S.C., Eglinton, G., Green, J.C., 1990. Long-chain alkenones and alkyl alkenoates and the fossil coccolith record of marine sediments. Chemical Geology 88, 349-375.

Martinez-Garcia, A., Rosell-Mele, A., Jaccard, S.L., Geibert, W., Sigman, D.M., Haug, G.H., 2011. Southern Ocean dust-climate coupling over the past four million years. Nature 476, 312-315.

Martinez-Garcia, A., Rosell-Mele, A., McClymont, E.L., Gersonde, R., Haug, G.H., 2010. Subpolar Link to the Emergence of the Modern Equatorial Pacific Cold Tongue. Science 328, 1550-1553.

Masson-Delmotte, V., Stenni, B., Pol, K., Braconnot, P., Cattani, O., Falourd, S., Kageyama, M., Jouzel, J., Landais, A., Minster, B., Barnola, J.M., Chappellaz, J., Krinner, G., Johnsen, S., Röthlisberger, R., Hansen, J., Mikolajewicz, U., Otto-Bliesner, B., 2010. EPICA Dome C record of glacial and interglacial intensities. Quaternary Science Reviews 29, 113-128.

McClymont, E.L., Rosell-Melé, A., 2005. Links between the onset of modern Walker Circulation and the mid-Pleistocene climate transition. Geology 33, 389-392.

McClymont, E.L., Rosell-Mele, A., Giraudeau, J., Pierre, C., Lloyd, J.M., 2005. Alkenone and coccolith records of the mid-Pleistocene in the south-east Atlantic: Implications for the U^{K}_{37}' index and South African climate. Quaternary Science Reviews 24, 1559-1572.

McClymont, E.L., Rosell-Mele, A., Haug, G.H., Lloyd, J.M., 2008. Mid-Pleistocene expansion of subarctic water masses in the northern Atlantic and Pacific Oceans and their potential modulation of northern hemisphere ice-sheet growth. Paleoceanography, doi:10.1029/2008PA001622.

Medina-Elizalde, M., Lea, D.W., 2005. The Mid-Pleistocene Transition in the Tropical Pacific. Science 310, 1009-1012.

Mudelsee, M., Schulz, M., 1997. The Mid-Pleistocene climate transition: onset of 100ka cycle lags ice volume build-up by 280ka. Earth and Planetary Science Letters 151, 117-123.

Mudelsee, M., Stattegger, K., 1997. Exploring the structure of the mid-Pleistocene Revolution with advanced methods of time-series analysis. Geologische Rundschau 86, 499-511.

Müller, P.J., Kirst, G., Ruhland, G., Storch, I.V., Rosell-Melé, A., 1998. Calibration of the alkenone paleotemperature index U^{k}_{37}' based on core-tops from the eastern South Atlantic and the global ocean (60°N–60°S). Geochimica et Cosmochimica Acta 62, 1757–1772.

Paillard, D., 1998. The timing of Pleistocene glaciations from a simple multiple-state climate model. Nature 391, 378-381.

Petrick, B.F., McClymont, E.L., Marret, F., in prep. Interaction between the Agulhas Leakage and the Benguela upwelling system over the last 1.5 Ma. Paleoceanography.

Pflaumann, U., Sarnthein, M., Ficken, K., Grothmann, A., Winkler, A., 1998. Variations in eolian and carbonate sedimentation, sea-surface temperature, and productivity over the last 3 m.y. at Site 958 off northwest Africa, In: Firth, J.V. (Ed.), Proceedings of the Ocean Drilling Program, Scientific Results, vol. 159T. College Station, TX (Ocean Drilling Program), pp. 3-16.

Pollard, D., DeConto, R.M., 2009. Modelling West Antarctic ice sheet growth and collapse through the past five million years. Nature 458, 329-332.

Prahl, F.G., Muehlhausen, L.A., Zahnle, D.I., 1988. Further evaluation of long-chain alkenones as indicators of paleoceanographic conditions. Geochimica et Cosmochimica Acta 52, 2303-2310.

Prahl, F.G., Wakeham, S.G., 1987. Calibration of unsaturation patterns in long-chain ketone compositions for palaeotemperature assessment. Nature 320, 367-369.

Ravelo, A.C., Andreasen, D.H., Lyle, M., Olivarez Lyle, A., Wara, M.W., 2004. Regional climate shifts caused by gradual global cooling in the Pliocene epoch. Nature 429, 263-267.

Raymo, M.E., 1997. The timing of major climate terminations. Paleoceanography 12, 577-585.

Raymo, M.E., Lisiecki, L.E., Nisancioglu, K.H., 2006. Plio-Pleistocene Ice Volume, Antarctic Climate, and the Global {delta}18O Record. Science 313, 492-495.

Raymo, M.E., Oppo, D.W., Curry, W., 1997. The mid-Pleistocene climate transition: A deep sea carbon isotope perspective. Paleoceanography 12, 546-559.

Raymo, M.E., Oppo, D.W., Flower, B.P., Hodell, D.A., McManus, J.F., Venz, K.A., Kleiven, K.F., McIntyre, K., 2004. Stability of North Atlantic water masses in face of pronounced climate variability during the Pleistocene. Paleoceanography 19, PA2008, doi:2010.1029/2003PA000921.

Rodríguez-Sanz, L., Graham Mortyn, P., Martínez-Garcia, A., Rosell-Melé, A., Hall, I.R., 2012. Glacial Southern Ocean freshening at the onset of the Middle Pleistocene Climate Transition. Earth and Planetary Science Letters 345–348, 194-202.

Rosell-Melé, A., Martínez-Garcia, A., McClymont, E.L., under review. Persistent Benguela "El Niño"-like conditions during the warm Pliocene epoch. Earth and Planetary Science Letters.

Rosenthal, Y., 2007. Elemental Proxies for Reconstructing Cenozoic Seawater Paleotemperatures, In: Hillaire-Marcel, C., De Vernal, A. (Eds.), Proxies in Late Cenozoic Paleoceanography. Elsevier, pp. 765-798.

Rosenthal, Y., Lohmann, G., Lohmann, K.C., Sherrell, R.M., 2000. Incorporation and preservation of Mg in *Globerigenoides sacculifer:* implications for reconstructing the temperature and $^{18}O/^{16}O$ of seawater. Paleoceanography 15, 135-145.

Rosenthal, Y., Lohmann, G.P., 2002. Accurate estimation of sea surface temperatures using dissolution-corrected calibrations for Mg/Ca paleothermometry. Paleoceanography 17, 1044, doi:1010.1029/2001PA000749.

Ruddiman, W.F., 2006. Orbital changes and climate. Quaternary Science Reviews 25, 3092-3112.

Ruddiman, W.F., McIntyre, A., Raymo, M.E., 1986. Paleoenvironmental Results from North Atlantic Sites 607 and 609, In: Ruddiman, W.F., Kidd, R.B., Thomas, E., etal (Eds.), Initial Reports, DSDP 94. U.S. Govt. Printing Office, Washington, pp. 855-878.

Ruddiman, W.F., Raymo, M.E., Martinson, D.G., Clement, B.M., Backman, J., 1989. Pleistocene evolution: northern hemisphere ice-sheets and north Atlantic Ocean. Paleoceanography 4, 353-412.

Russon, T., Elliot, M., Sadekov, A., Cabioch, G., Corrège, T., De Deckker, P., 2010. Inter-hemispheric asymmetry in the early Pleistocene Pacific warm pool. Geophysical Research Letters 37, L11601.

Sancetta, C., Silvestri, S., 1986. Pliocene-Pleistocene evolution of the North Pacific ocean-atmosphere system, interpreted from fossil diatoms. Paleoceanography 1, 163-180.

Sawada, K., Handa, N., Nakatsuka, T., 1998. Production and transport of long-chain alkenones and alkyl alkenoates in a sea water column in the northwestern Pacific off central Japan. Marine Chemistry 59, 219-234.

Schefuß, E., Schouten, S., Jansen, J.H.F., Sinninghe Damsté, J.S., 2003. African vegetation controlled by tropical sea surface temperatures in the mid-Pleistocene period. Nature 422, 416-421.

Schefuß, E., Sinninghe Damsté, J.S., Jansen, J.H.F., 2004. Forcing of tropical Atlantic sea surface temperatures during the mid-Pleistocene transition. Paleoceanography 19, PA4029, doi:4010.1029/2003PA000892.

Scherer, R.P., Bohaty, S.M., Dunbar, R.B., Esper, O., Flores, J.A., Gersonde, R., Harwood, D.M., Roberts, A.P., Taviani, M., 2008. Antarctic records of precession-paced insolation-driven warming during early Pleistocene Marine Isotope Stage 31. Geophysical Research Letters 35, L03505.

Schmieder, F., von Dobeneck, T., Bleil, U., 2000. The Mid-Pleistocene climate transition as documented in the deep South Atlantic Ocean: initiation, interim state and terminal event. Earth and Planetary Science Letters 179, 539-549.

Sejrup, H.P., Larsen, E., Landvik, J., King, E.L., Haflidason, H., Nesje, A., 2000. Quaternary glaciations in southern Fennoscandia: evidence from southwestern Norward and the northern North Sea region. Quaternary Science Reviews 19, 667-685.

Seki, O., Foster, G.L., Schmidt, D.N., Mackensen, A., Kawamura, K., Pancost, R.D., 2010. Alkenone and boron-based Pliocene pCO2 records. Earth and Planetary Science Letters 292, 201-211.

Sexton, P.F., Barker, S., 2012. Onset of 'Pacific-style' deep-sea sedimentary carbonate cycles at the mid-Pleistocene transition. Earth and Planetary Science Letters 321–322, 81-94.

Shackleton, N.J., Berger, A., Peltier, W.R., 1990. An alternative astronomical calibration of the lower Pleistocene timescale based on ODP Site 677. Transactions of the Royal Society of Edinburgh, Earth Sciences 81, 251-261.

Sigman, D.M., Boyle, E.A., 2000. Glacial / Interglacial variations in atmospheric carbon dioxide. Nature 407, 859-869.

Sigman, D.M., Hain, M.P., Haug, G.H., 2010. The polar ocean and glacial cycles in atmospheric CO_2 concentration. Nature 466, 47–55.

Sime, N.G., De La Rocha, C.L., Tipper, E.T., Tripati, A., Galy, A., Bickle, M.J., 2007. Interpreting the Ca isotope record of marine biogenic carbonates. Geochimica et Cosmochimica Acta 71, 3979-3989.

Singer, B.S., Ackert, R.P., Guillou, H., 2004. $^{40}Ar/^{39}Ar$ and K-Ar chronology of Pleistocene glaciations in Patagonia. Geological Society of America Bulletin 116, 434-450.

Solheim, A., Faleide, J.I., Andersen, E.S., Elverhøi, A., Forsberg, C.F., Vanneste, K., Uenzelmann-Neben, G., 1998. Late Cenozoic seismic stratigraphy and glacial geological development of the east Greenland and Svalbard-Barents Sea Continental Margin. Quaternary Science Reviews 17, 155–185.

Sosdian, S., Rosenthal, Y., 2009. Deep-Sea Temperature and Ice Volume Changes Across the Pliocene-Pleistocene Climate Transitions. Science 325, 306-310.

Sun, Y., Clemens, S.C., An, Z., Yu, Z., 2006. Astronomical timescale and palaeoclimatic implication of stacked 3.6-Myr monsoon records from the Chinese Loess Plateau. Quaternary Science Reviews 25, 33-48.

Thierens, M., Pirlet, H., Colin, C., Latruwe, K., Vanhaecke, F., Lee, J.R., Stuut, J.B., Titschack, J., Huvenne, V.A.I., Dorschel, B., Wheeler, A.J., Henriet, J.P., 2012. Ice-rafting from the British-Irish ice sheet since the earliest Pleistocene (2.6 million years ago): implications for long-term mid-latitudinal ice-sheet growth in the North Atlantic region. Quaternary Science Reviews 44, 229-240.

Thompson, P.R., 1981. Planktonic foraminifera in the western North Pacific during the past 150,000 years: Comparison of modern and fossil assemblages. Palaeogeography, Palaeoclimatology, Palaeoecology 35, 241-279.

Toggweiler, J.R., Russell, J.L., Carson, S.R., 2006. Midlatitude westerlies, atmospheric CO_2, and climate change during the ice ages. Paleoceanography 21, PA2005, doi:2010.1092/2005PA001154.

Trauth, M.H., 2007. MATLAB Recipes for Earth Sciences. Second Edition, Springer.

Tziperman, E., Gildor, H., 2003. On the mid-Pleistocene transition to 100-ky glacial cycles and the asymmetry between glaciation and deglaciation times. Paleoceanography 18, 1-8.

Van de Wal, R.S.W., Bintanja, R., 2009. Changes in Temperature, Ice, and CO2 During the Mid-Pleistocene Transition. Science, e-letter comment, 18th September 2009.

Vincent, E., Berger, W.H., 1981. Planktonic foraminifera and their use in Paleoceanography, In: Emiliani, C. (Ed.), The oceanic lithosphere. The sea. Hoboken, N.J.: Wiley Interscience, pp. 1025-1119.

Volkman, J.K., Barrett, S.M., Blackburn, S.I., Sikes, E.L., 1995. Alkenones in *Gephyrocapsa oceanica*: Implications for studies of paleoclimate. Geochimica et Cosmochimica Acta 59, 513-520.

Volkman, J.K., Eglington, G., Corner, E.D.S., Forsberg, T.E.V., 1980. Long-chain alkenes and alkenones in the marine coccolithophorid *Emiliania huxleyi*. Phytochemistry 19, 2619–2622.

Wara, M.W., Ravelo, A.C., Delaney, M.L., 2005. Permanent El Nino-Like Conditions During the Pliocene Warm Period. Science 309, 758-761.

Watson, A.J., Bakker, D.C.E., Ridgwell, A.J., Boyd, P.W., Law, C.S., 2000. Effect of iron supply on Southern Ocean CO_2 uptake and implications for glacial atmospheric CO_2. Nature 407, 730-733.

Watson, A.J., Naveira Garabato, A.C., 2006. The role of Southern Ocean mixing and upwelling in glacial-interglacial atmospheric CO_2 change. Tellus 58B, 73-87.

Yin, Q.Z., Berger, A., 2010. Insolation and CO2 contribution to the interglacial climate before and after the Mid-Brunhes Event. Nature Geosci 3, 243-246.

Figure legends

Figure 1. Map of sites presented here, superimposed upon mean annual SSTs as detailed by the World Ocean Atlas (2005). For full details of original publications and age model construction see Table 1. Data sets are shown as black circles (U^{K}_{37}' index), white circles (Mg/Ca in planktonic foraminifera), white triangles (planktonic foraminifera transfer functions) or multi-proxy (grey diamond).

Figure 2 Pleistocene sea-surface temperature trends as recorded by low bandpass filters (200 ka) and displayed as the anomaly from the maximum SST value identified in the 2 Ma time window. Sub-orbital SST variability exceeds the magnitude of these trends. Original data sources for each site are shown in Table 1. The benthic oxygen isotope stack (LR04, Lisiecki and Raymo, 2005) and the deep water temperature records from the north Atlantic (DWT-A) (Sosdian and Rosenthal, 2009) and SW Pacific (DWT-P)(Elderfield et al., 2012) are shown in the upper panel. The zone of common cooling intensification is highlighted by the vertical yellow bar. Note that the y-axis scale for the high latitudes (northern hemisphere) is compressed relative to the others.

Figure 3 SiZer maps detailing the patterns of change in selected SST records. Each map is produced as a result of repeated smoothed curves being fitted to the data at a series of bandwidths (Chaudhuri and Marron, 1999). In each case the curve is tested for deviation from a gradient of zero. The y-axis gives the bandwidth (as log10(h) such that log10(h)=2 represents the 200 ka bandwidth). Trends are identified by shading in: blue (significant decrease), red (significant increase), purple (no trend) and grey (insufficient

data to make a definitive conclusion). The two dashed lines illustrate the width of the smoothing window used for each bandwidth. For example, if the ODP 846 SST record is considered, the SiZer map reveals an overall cooling at long timescales (continuous blue above log10(h)=2.5) but also the presence of shorter term variability (likely glacial-interglacial cycles) shown by repeated fluctuations between blue and red at log10(h) <1.5.

Figure 4 Interglacial trends (normalized) derived from sea surface temperature records from (a) tropical latitudes, (b) high northern and southern latitudes, and mid northern latitudes. Panel (c) shows the interglacial values recorded in insolation at 65°N and 65°N (Berger and Loutre, 1991), the LRO4 $\delta^{18}O_b$ stack (Lisiecki and Raymo, 2005), Fe-mass accumulation rates at ODP 1090 (Martinez-Garcia et al., 2011), and pCO_2 concentrations from the EPICA ice core (Luthi et al., 2008). The average interglacial CO_2 concentrations reconstructed from the $\delta^{11}B$ proxy (Hönisch et al., 2009) are marked by the dashed lines.

Figure 5 Glacial trends (normalized) derived from sea surface temperature records and other climate indicators. See Figure 4 for a full description of the archives used.

Figure 6 Wavelet power spectra for SST records spanning the last 2 Ma, and the $\%C_{37:4}$ alkenone record from ODP 1090 (Subantarctic Atlantic). All records were linearly interpolated to the average sample spacing of the record concerned, and

processed following the WTC-16 Matlab code of Grinsted *et al.* (2004). Spectral power is indicated by the color bar on the right of each output. Variability at the precession (P), obliquity (O) and eccentricity (E) periods are highlighted. The solid black contour lines identify regions where spectral power meets the 5% significance level against red noise. Pale shading identifies the cone of influence where edge effects in processing may impact the signal.

Figure 7 Original data sets plotted for selected time intervals. Part A (left) shows the last 3 100 ka glacial cycles, Part B (right) includes the "premature" 100 ka cycle at 1.2 Ma (vertical yellow bar) and the cool interval of MIS 24-22 or the "900 ka event" (vertical yellow bar). Orbital parameters are from Berger and Loutre (1991). The horizontal green bar on each record shows the cool SST observed during the premature 100 ka cycle, for comparison to later glacial stages.

Figure 8 Conceptual outline of SST trends for the last 2 Ma. Interglacial trends are marked by dashed lines, glacial trends are marked by solid lines. Also shown are trends in the benthic $\delta^{18}O$ stack (Lisiecki and Raymo, 2005), bottom water temperatures from the north Atlantic (Sosdian and Rosenthal, 2009) and SW Pacific (Elderfield et al., 2012), dust inputs to the Subantarctic Atlantic (Martinez-Garcia et al., 2011), and pCO_2 as recorded in the EPICA ice core (Luthi et al., 2008). Lower resolution pCO_2 trends prior to 1.0 Ma reflect the data from Hönisch et al. (2009). The duration of the MPT is noted according to Mudelsee and Schulz (1997; MS97) or Clark et al. (2006; C06).

Table 1 Site locations for those records re-analysed by one or more treatments here. Age models: specified proxy tuned to LR04 (Lisiecki and Raymo, 2005), Sh677 (Shackleton et al., 1990), BL91 (Berger and Loutre, 1991), or La (Laskar, 1990). "GRAPE" refers to the gamma-ray attenuation porosity evaluator recorded in sediments, which reflects sediment density and can be used to record climate-related properties such as carbonate content. For foraminifera transfer functions the following approaches are noted: * FP-12E linear transfer function (Thompson, 1981), § Artificial neural network (Crundwell et al., 2008), ‡ (Imbrie and Kipp, 1971).

Location	Site	Latitude, Longitude	Water Depth (km)	Original age model	Mean resolution (ka)	SST proxy	Original reference
Arabian Sea	ODP722	16°37'N, 59°48'E	2.022	Benthic $\delta^{18}O$ (LR04)	1.9	U^{K}_{37}'	(Herbert et al., 2010)
South China Sea	GIK17957-2	10.9°N, 115.3ºE	2.195	Benthic $\delta^{18}O$ (Sh677)	5.4	Planktonic foraminifera transfer function *	(Jian et al., 2000)
	IODP 1143	9°22'N, 113°17'E	2.772	Benthic $\delta^{18}O$ (La)	3.0	U^{K}_{37}'	(Li et al., 2011)
	IODP1146	19°27'N, 116°16'E	2.092	Benthic $\delta^{18}O$ (LR04)	1.7	U^{K}_{37}'	(Herbert et al., 2010)
West Pacific Warm Pool	MD97-2140	2°02'N, 141°46'E	2.547	Benthic $\delta^{18}O$ (Sh677)	4.9	Mg/Ca in *G. ruber* (250-300 mm, white)	(de Garidel-Thoron et al., 2005)
	ODP806	0°19.1'N, 159°21.7'E	2.520	Benthic $\delta^{18}O$ (Sh677)	2.4	Mg/Ca in *G. ruber*	(Medina-Elizalde and Lea, 2005)

	ODP806	0°19.1'N, 159°21.7'E	2.520	Benthic $\delta^{18}O$ (Sh677)	17.4	Mg/Ca in *G. sacculifer*	(Wara et al., 2005)
Coral Sea	MD06-3018	23°00′S, 166°09′E	2.470	Benthic $\delta^{18}O$ (LR04)	5.9	Mg/Ca in *G. ruber*	(Russon et al., 2010)
SW Pacific	ODP1123	41°47.2'S, 171°29.9'W	3.290	Benthic $\delta^{18}O$ (Imbrie93)	2.4	Planktonic foraminifera transfer function § Benthic foraminifera Mg/Ca temperatures	Crundwell *et al.* (2008) (Elderfield et al., 2012)
East equatorial Pacific	ODP846	3°6'S, 90°49'W	3.295	Benthic $\delta^{18}O$ (LR04)	2.3	U^{K}_{37}'	(Lawrence et al., 2006)
	ODP847	0°12'N, 95°19'W	3.346	Benthic $\delta^{18}O$ (Sh677)	21.2	Mg/Ca in *G. sacculifer*	(Wara et al., 2005)
	ODP847	0°12'N, 95°19'W	3.346	GRAPE (BL91)	12.6	U^{K}_{37}'	(Dekens et al., 2007)
	ODP849	0°11'N, 110°31'W	3.839	Benthic $\delta^{18}O$ (Sh677)	5.5	U^{K}_{37}'	(McClymont and Rosell-Melé, 2005)
California margin	ODP1012	32°17'N, 118°24'W	1.772	Benthic $\delta^{18}O$ (LR04)	2.0	U^{K}_{37}'	(Liu et al., 2005)
	ODP1014	32°50'N, 119°59'W	1.165	Benthic $\delta^{18}O$ (BL91)	11.7	U^{K}_{37}'	(Dekens et al., 2007)
	ODP1020	41°0'N, 126°26'W	3.050	Benthic $\delta^{18}O$ (LR04)	2.0	U^{K}_{37}'	Liu (2004)

Peru margin	ODP1237	16°0'S, 76°23'W	3.212	Biostrat (ODP)	10.8	U^{K}_{37}'	(Dekens et al., 2007)
Tropical and subtropical Atlantic	ODP662	1°23.412'S, 11°44.352'W	3.814	Benthic $\delta^{18}O$ (LR04)	3.9	U^{K}_{37}'	(Herbert et al., 2010)
	ODP1077	5°11'S, 10°26'E	2.382	Benthic $\delta^{18}O$ (Sh677)	3.8	U^{K}_{37}'	(Schefuß et al., 2004)
Benguela upwelling	ODP1081	19°37'S, 11°19'E	0.794	Benthic $\delta^{18}O$ (BL91)	13.0	U^{K}_{37}'	(Durham et al., 2001; Marlow, 2001)
	ODP1082	21°5′S, 11°49′E	1.280	Benthic $\delta^{18}O$ (LR04)	4.7	U^{K}_{37}'	(Etourneau et al., 2009)
	ODP1084	25°31'S, 13°2'E	1.992	Biostrat (ODP)	40.5	U^{K}_{37}'	(Marlow et al., 2000)
	ODP1087	31°28'S, 15°19'E	1.372	Benthic $\delta^{18}O$ (BL91)	5.5	U^{K}_{37}'	(Marlow, 2001; McClymont et al., 2005)
Southern Ocean	ODP 1090	42º54.8'S, 8º53.9'E	3.700	Benthic $\delta^{18}O$ (LR04)	2.6	U^{K}_{37} and U^{K}_{37}'	(Martinez-Garcia et al., 2010)
North Atlantic	ODP 607	41°00'N, 32°58'W	3.427	Benthic $\delta^{18}O$ (LR04)	3.9	Planktonic foraminifera ‡ U^{K}_{37}' Benthic foraminifera Mg/Ca temperatures	(Ruddiman et al., 1989) (Lawrence et al., 2011) (Sosdian and Rosenthal, 2009)

	ODP 982	57°30'N, 15°52'W	1.134	Benthic $\delta^{18}O$ (LR04)	5.0	U^{K}_{37}'	(Lawrence et al., 2009)
	ODP 983	60°24'N, 23°38'W	1.985	Benthic $\delta^{18}O$ (Sh677)	5.4	U^{K}_{37} and U^{K}_{37}'	(McClymont et al., 2008)
North west Pacific	ODP882	50°21'N, 167°35'W	3.244	GRAPE (BL91)	6.5	U^{K}_{37}'	(Martinez-Garcia et al., 2010)

Table 2 SST anomalies relative to the "41 ka world" (1.3 – 1.8 Ma) for those sites outlined in Table 1 which span the Pleistocene. Anomalies are calculated using the mean annual SST values recorded for each of the time intervals noted here. Data sets are annotated according to whether they record winter (w) or summer (s) SSTs, deep-water temperatures (*DWT*), or were produced by Medina-Elizalde (M), Dekens (D) or Wara (W). For full details see Table 1. If the anomaly exceeds the calibration error of the proxy concerned the box is shaded.

Location	**Site**	**41 ka mean (1.3 – 1.8 Ma)**	**Anomalies relative to 41 ka mean**		
			100 ka (0 – 0.43 Ma)	**Late MPT (0.6 – 0.8 Ma)**	**Early MPT (1.1 – 0.9 Ma)**
Arabian Sea	ODP 722	27.2	-1.30	-0.50	-0.12
South China Sea	GIK 17957-2	29.0 (s) 26.0 (w)	-0.39 (s) -0.54 (w)	-0.35 (s) -0.98 (w)	-0.19 (s) -0.03 (w)
	IODP 1146	26.7	-1.97	-1.16	-0.58
West Pacific Warm Pool	MD97-2140	29.4	-0.33	-0.21	-0.26
	ODP 806(M)	28.3	-0.41	-0.19	-0.38
	ODP 806(W)	28.0	-0.31	**+0.58**	**+0.83**
East equatorial Pacific	ODP 846	23.5	-1.74	-1.05	-0.13
	ODP 847(D)	25.1	-1.73	-0.46	-0.52
	ODP 847(W)	24.6	-1.03	+0.28	-0.66
California margin	ODP 1012	17.4	-1.89	-0.75	-0.14
	ODP 1014	17.1	**-2.02**	-1.47	+0.087
	ODP 1020	11.7	**-2.81**	-1.74	**-2.03**
Peru margin	ODP 1237	21.7	**-2.14**	**-2.18**	-0.05
Tropical Atlantic	ODP 662	26.4	-1.16	**-2.20**	-0.35

Benguela upwelling	ODP 1081	22.9	**-4.73**	**-3.70**	-0.87
	ODP 1082	22.4	**-3.78**	**-3.53**	-1.44
	ODP 1084	19.7	**-4.53**	**-5.59**	-1.36
	ODP 1087	18.4	**+0.54**	-1.97	-1.23
Southern Ocean	ODP 1090	11.5 (U^{K}_{37}')	-1.38	-1.44	-1.77
		11.3 (U^{K}_{37})	-0.72	-2.21	**-3.81**
North Atlantic	ODP 607 (r)	21.4 (s)	**-2.10**	**-3.52**	**+1.00**
		14.4 (w)	-1.67	**-3.16**	**+0.97**
	ODP 607 (DWT)	*2.30*	*-1.24*	*-1.10*	*0.01*
	ODP 982	14.0	-1.30	-1.29	-0.29
NW Pacific	ODP 882	11.1	**-2.46**	**-3.60**	**-2.86**

Table 3 Statistical analysis of SST mean, interglacial, and glacial trends. T, temperature in degrees Celsius; r, correlation coefficient; t, age in thousands of years. Relationships are shaded and in bold where r>0.4.

			Linear trend	
Site	**Time span**	**SST (entire series)**	**Interglacials**	**Glacials**
High northern latitudes				
ODP 982	0 - 2.0 Ma	T=12.5 + 0.0008 t r=0.29	T=13.9 + 0.0005 t r=0.25	**T=10.6 + 0.0015 t** **r=0.53**
Mid northern latitudes				
DSDP 607	0.25 - 2.0Ma	**T=14.3 + 0.0022 t** **r=0.52**	**T=14.3 + 0.0022 t** **r=0.52**	**T=14.3 + 0.0022 t** **r=0.52**
ODP 1020	0 - 1.64 Ma	**T=8.0 + 0.0022 t** **r=0.47**	**T=11.4+ 0.0014 t** **r=0.45**	**T=6.15 + 0.0019 t** **r=0.59**
Tropical latitudes				
ODP 722	0 - 2.0 Ma	T=25.9 + 0.00075 t r=0.42	T=27.7- 0.0001 t r=-0.12	**T=24.9+ 0.001 t** **r=0.56**
ODP 1146	0 - 2.0 Ma	**T=24.4 + 0.0015 t** **r=0.65**	T=27.0 + 0.00034 t r=0.36	**T=23.1 + 0.0019 t** **r=0.76**
Western equatorial Pacific				
ODP 806	0 - 1.35 Ma	T=27.7 + 0.00042 t r=0.19	T=28.9+ 0.00001 t r=0.06	T=26.8+ 0.0063 t r=0.43
MD97-2140	0 – 1.755 Ma	T=29.2 + 0.00014 t r=0.08	T=30.6 - 0.0004 t r=-0.29	T=28.5+ 0.00028 t r=0.18
Upwelling regimes				
ODP 846	0 - 2.0 Ma	**T=21.9 + 0.0011 t** **r=0.57**	T=23.7 + 0.00042 t r=0.28	**T=20.7 + 0.0014 t** **r=0.69**
ODP 1012	0 – 1.812 Ma	T=15.4 + 0.0013 t r=0.37	T=18.4 + 0.00045 t r=0.24	T=13.8 + 0.0013 t r=0.43

Mid southern latitude				
ODP 1090	0 - 2.0 Ma	T=8.91 + 0.0014 t r=0.42	T=11.5 + 0.00035 t r=0.14	**T=7.45 + 0.0017 t** **r=0.47**
ODP 1123	0 - 1.2 Ma	T=15.9 - 0.00078 t r=-0.12	T=17.9 + 0.000045 t r=-0.02	T=12.8 - 0.00202 t r=--0.39
Other variables				
LRO4 $\delta^{18}O_b$	0 - 2.0 Ma	$\delta^{18}O_b$=4.25 - 0.00026t r=-0.36	$\delta^{18}O_b$ =3.3 + 0.0001 t r=0.33	**$\delta^{18}O_b$ =5.0 - 0.0005 t** **r=-0.86**
Dust: Fe MAR	0 - 2.0 Ma	Fe MAR=249- 0.070 t r=0.33	Fe MAR=89.3 - 0.0045 t r=-0.09	**Fe MAR=531 - 0.22 t** **r=-0.72**
Ice core pCO_2	0 - 0.8 Ma	pCO_2=244-0.035 t r=0.33	**pCO_2=287.4 - 0.050 t** **r=-0.63**	pCO_2=186.9 - 0.0013 t r=-0.03

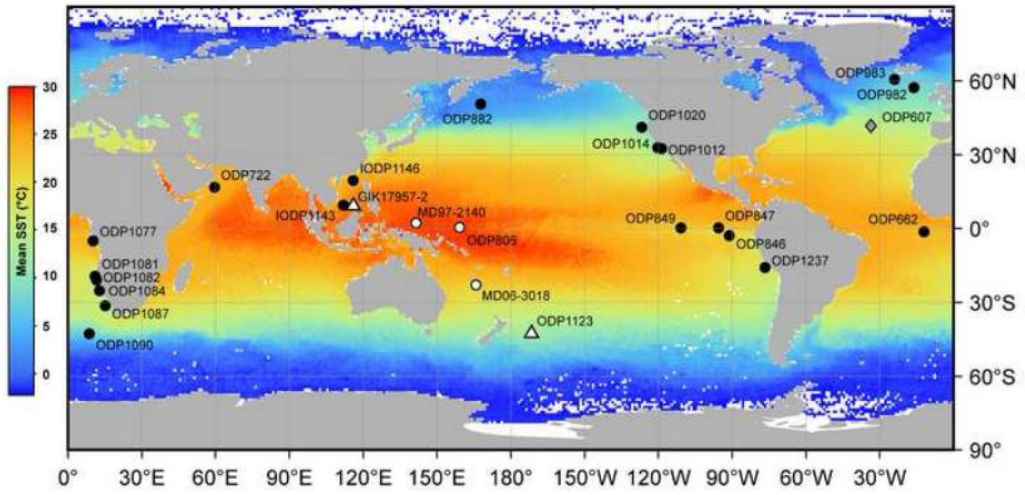

Figure 1

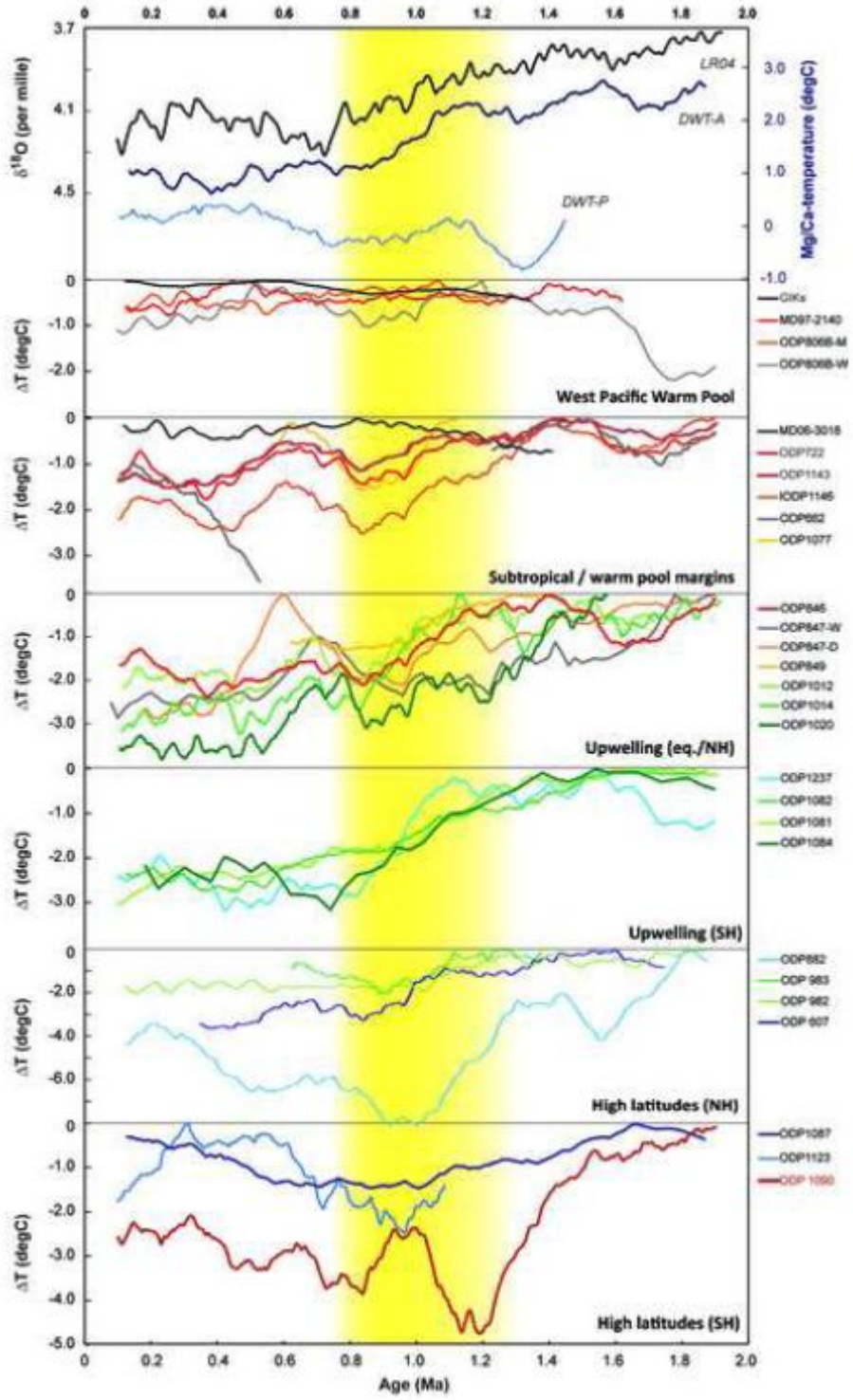
δ18O (per mille)
LR04
DWT-A
DWT-P
Mg/Ca-temperature (degC)
ΔT (degC)
West Pacific Warm Pool
Subtropical / warm pool margins
Upwelling (eq./NH)
Upwelling (SH)
High latitudes (NH)
High latitudes (SH)
Age (Ma)

Figure 2

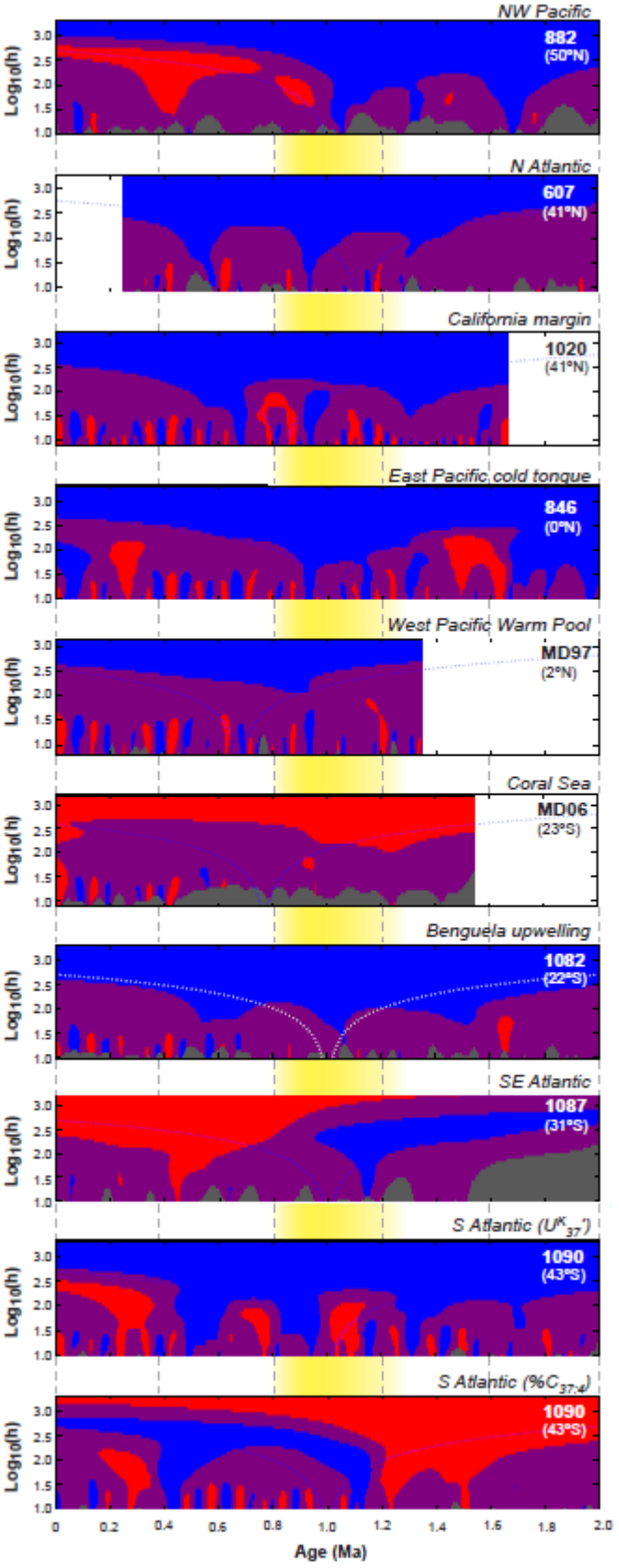

Figure 3

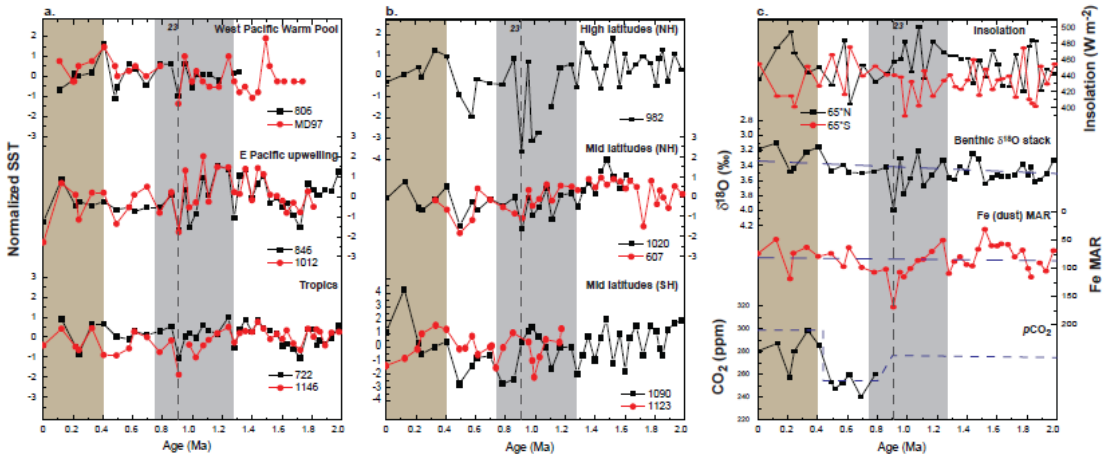

Figure 4

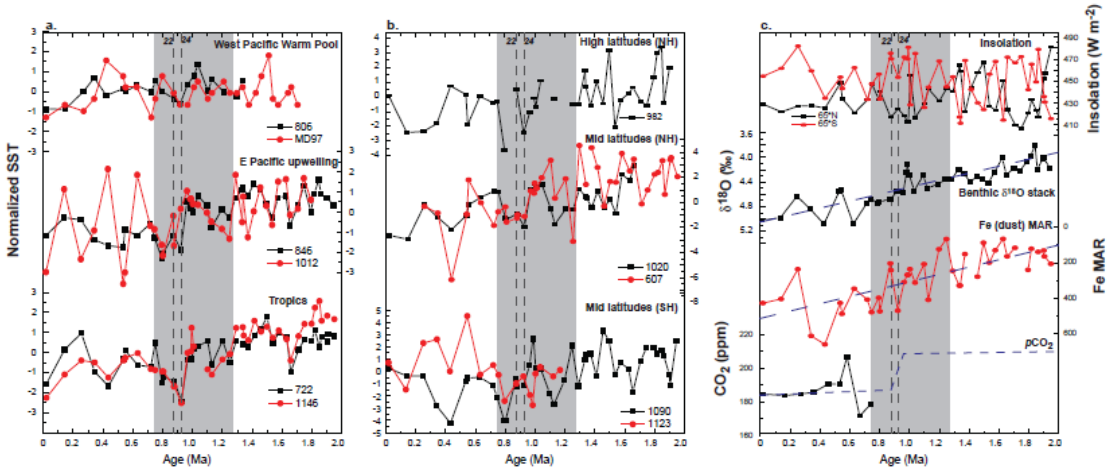

Figure 5

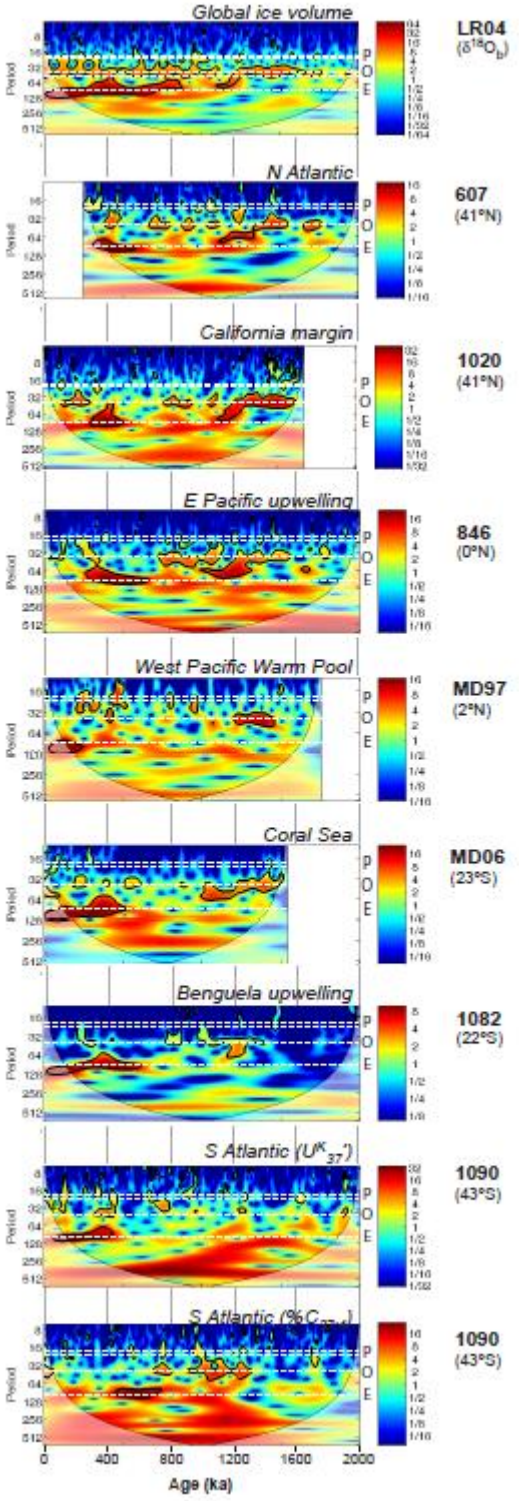

Figure 6

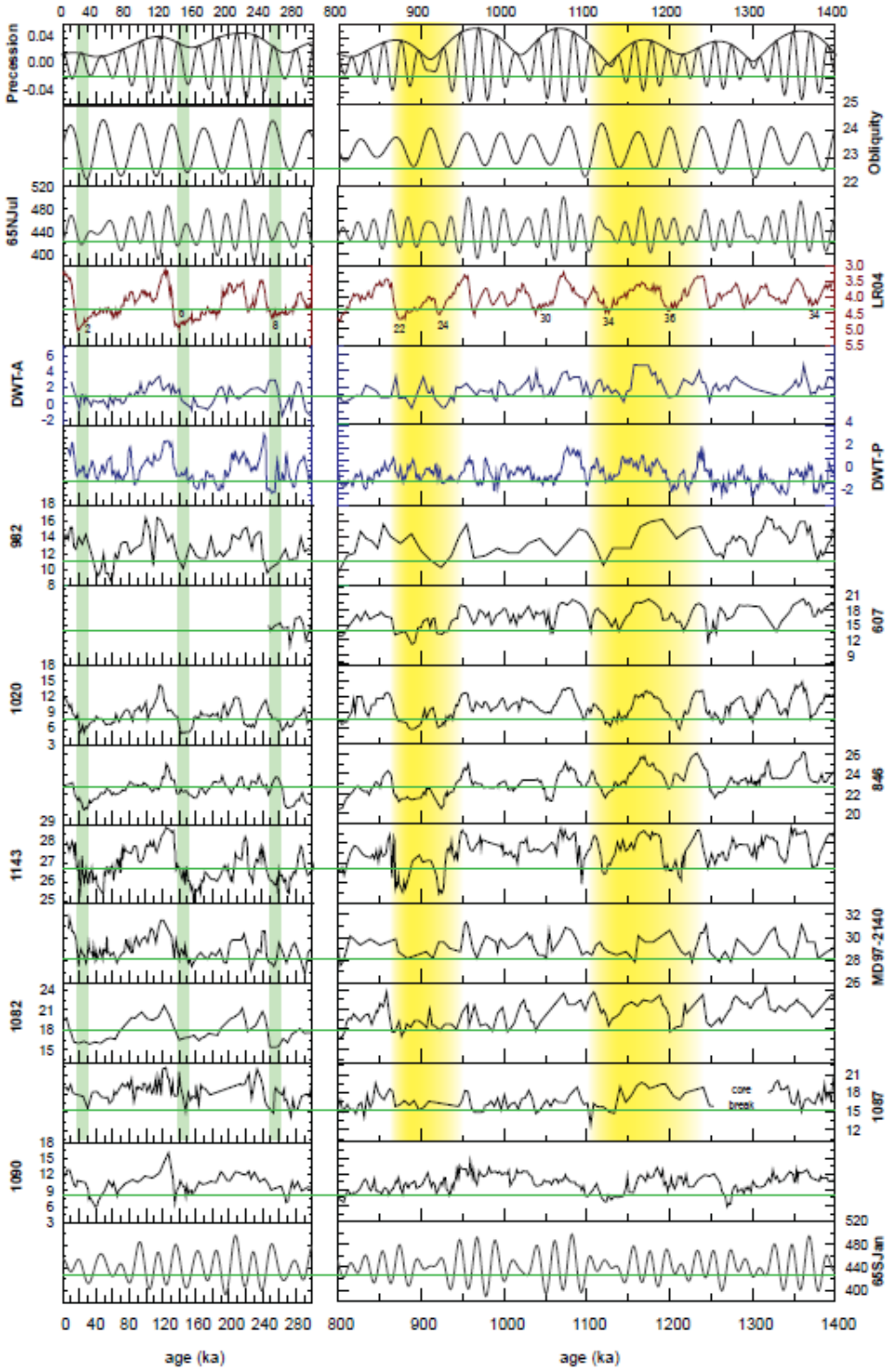

Figure 7

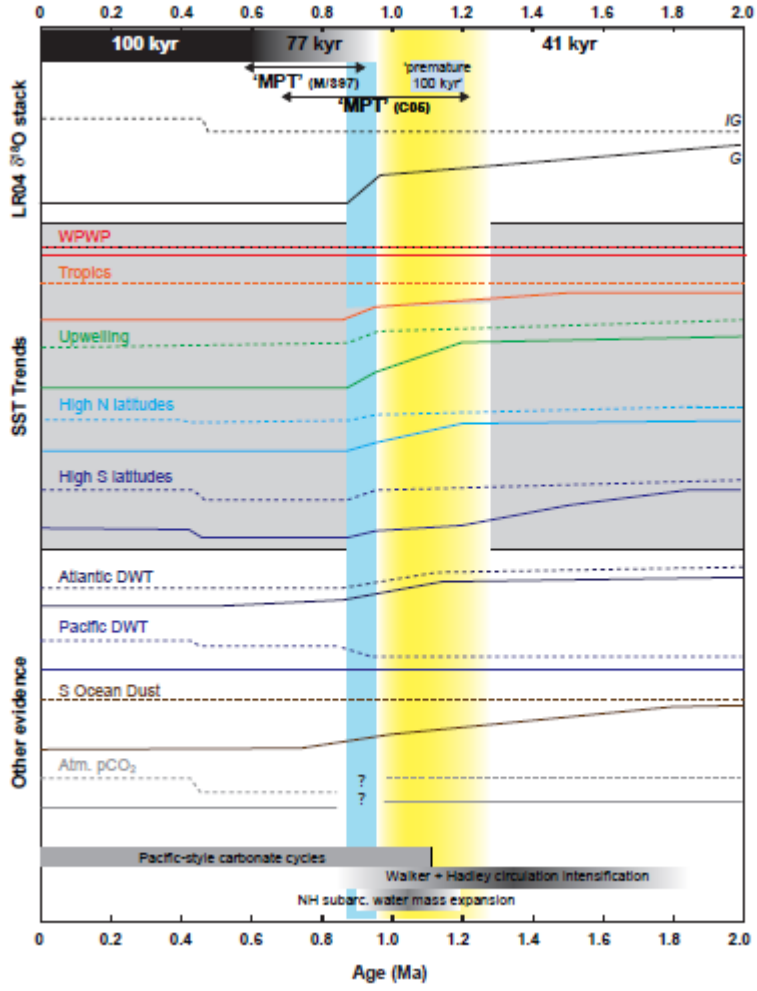

Figure 8